

Original paper

Mineralogy and genetic aspects of the metamorphosed manganese mineralization at the Július ore occurrence near Betliar (Gemic Unit, Western Carpathians, Slovakia)

Pavol MYŠLAN^{1,2*}, Martin ŠTEVKO^{1,3}, Tomáš MIKUŠ⁴¹ Earth Science Institute, Slovak Academy of Sciences, Dúbravská cesta 9, 840 05 Bratislava, Slovakia; pavol.myslan@savba.sk² Department of Mineralogy, Petrology and Economic Geology, Faculty of Natural Sciences, Comenius University, Ilkovičova 6, 842 15, Bratislava, Slovakia³ Department of Mineralogy and Petrology, National Museum, Cirkusová 1740, 193 00 Prague 9-Horní Počernice, Czech Republic⁴ Earth Science Institute, Slovak Academy of Sciences, Ďumbierska 1, 974 11 Banská Bystrica, Slovakia

*Corresponding author



The Július metamorphosed manganese occurrence is situated near the Betliar village in the Spišsko-gemerské rudohorie Mts. (Western Carpathians). Mineralization occurs in the form of manganese carbonate-silicate lenticular body hosted in Lower Paleozoic metasedimentary and metavolcanoclastic rocks of the Bystrý potok Formation, Gelnica Group, Gemic Unit. The Mn mineralization dominantly consists of rhodochrosite, pyroxmangite, spessartine, magnetite, clino-suenoite, clino-ferro-suenoite, tephroite, pyrophanite and pyrosmalite-(Mn) alongside with pyrite, pyrrhotite, galena, sphalerite, cobaltite, gersdorffite, siegenite, violarite and minor pentlandite and millerite. Very rare minerals, such as hejtmanite, bafertsite as well as two recently approved members of the epidote supergroup [ferriandrosite-(Ce) and vielleaureite-(Ce)] were also identified. Significant feature of studied mineralization in comparison with the other occurrences of metamorphosed manganese mineralization in the Spišsko-gemerské rudohorie Mts. is the absence of rhodonite. Mineralization at the Július occurrence originates from heterogeneous sediment with occurrence of manganese, calcareous, argillaceous and terrigenous material with quartz and Ba-rich minerals locally incorporated by material from a volcanic source. Based on mineralogy and ore textures, two metamorphic stages affecting the final mineral composition of Mn mineralization can be distinguished. Generally, the mineral assemblage was likely formed during the Variscan metamorphic stage in the p–T conditions approximately 420–450 °C and pressure 2–4 kbar, as a peak of a metamorphism can be considered the high-grade greenschist facies conditions. Alpine metamorphic phase determined the appearance of veins and veinlets composed of rhodochrosite–chamosite–quartz, pyroxmangite and spessartine. In agreement with lowering temperature of metamorphism and with higher mobility of REE, minerals such as epidotes, baryte and pyrosmalite-(Mn) were formed. Hydrothermal activity led to the formation of sulphides with slightly increased content of Mn. Final stage of metamorphic evolution was influenced by local metasomatic processes.

Keywords: manganese mineralization, rhodochrosite, pyroxmangite, Betliar, Gemic Unit, Slovakia

Received: 16 March 2023; **accepted:** 20 December 2023; **handling editor:** P. Jeřábek

The online version of this article (doi: 10.3190/jgeosci.384) contains supplementary electronic material (ESM).

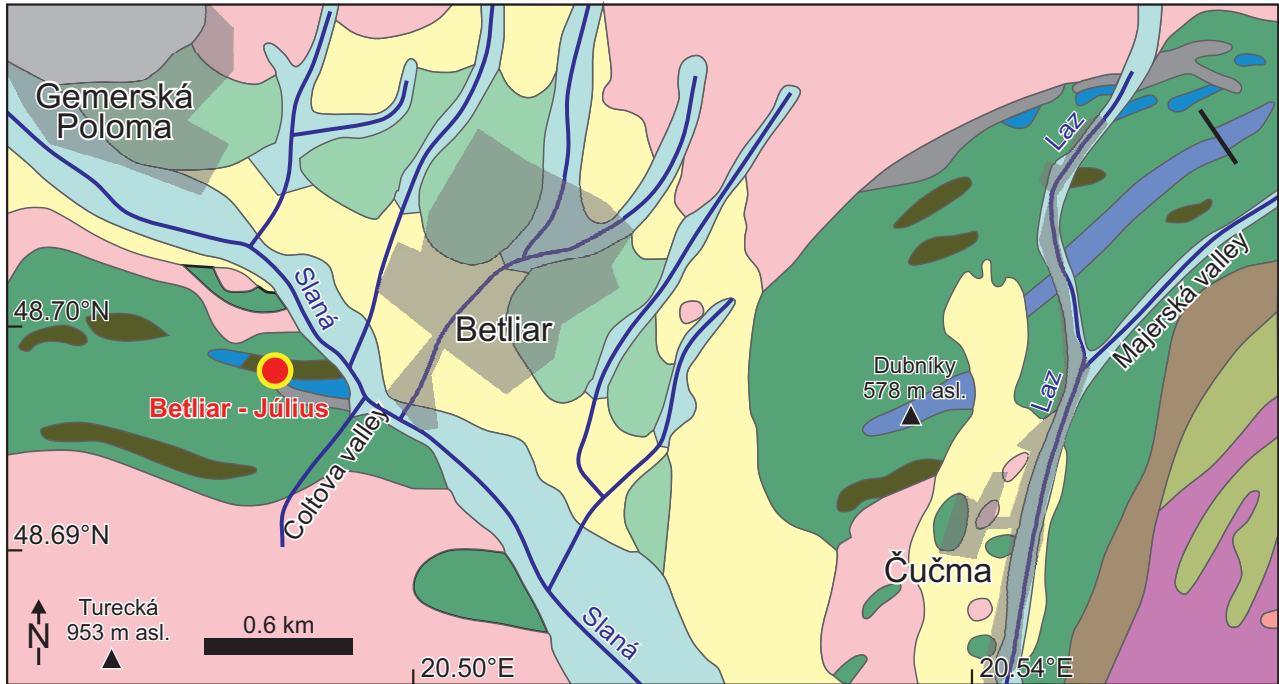
1. Introduction

Manganese mineralization is distributed in widespread geological environments around the world divided into different types according to their origin, evolution and element or mineral distribution (Laznicka 1992). For instance, based on protolith and genesis, most important manganese deposits can be classified as sedimentary, volcano–sedimentary, metamorphic, hydrothermally altered, hydrothermal and supergene (Fan, Yang 1999). The most variable mineral composition is mainly in metamorphosed deposits consisting of a large number of different minerals genetically linked to their polystadial development (Dasgupta et al. 1990; Melcher 1995; Nakagawa et al. 2009; Brusnitsyn et al. 2017).

As stated above, in the metamorphosed deposits a variable mineral association is present, which is consistent with the various mineral composition at the Spišsko-gemerské rudohorie Mts. localities situated in Slovakia. Occurrences of the metamorphosed Mn mineralization at the Spišsko-gemerské rudohorie Mts. were explored since 17th century at the localities Čučma–Čierna baňa, Malá Hekerová–Bystrý potok near Smolník and Betliar–Július (Maderspach 1875, 1880; Lázár 1959). Individual occurrences with interesting mineral assemblages were studied in limited quantity only at the Čučma and Malá Hekerová deposits, where silicate–carbonate lenses with manganese ore mineralization occur within greenschist facies of metavolcano–sedimentary rocks of the Gelnica Group in Gemic Unit. Their polygenetic origin is reflected

in different mineral assemblages consisting of approximately 80 minerals with most abundant primary minerals represented by rhodonite, rhodochrosite, Mn-rich calcite, pyroxmangite, tephroite, spessartine, pyrosmalite-(Mn), hausmannite, pyrophanite, ferri-gohseite, clino-suenoite and sulphides such as pyrite, pyrrhotite, chalcopyrite, arsenopyrite, galena, sphalerite, cobaltite, gersdorffite etc. (Maderspach 1880; Kantor 1953a, b; Gargulák et al. 1985; Faryad 1994; Rojkovič 2001; Peterec, Ďuša 2003, 2009; Števko et al. 2015; Radvanec, Gonda 2020).

Mineralogy of the Július metamorphosed manganese ore mineralization has never been studied in detail. Up to now, the mineral composition of ore bodies at the Betliar-Július was assumed to be composed of mainly of rhodonite with high Ca content associated with rhodochrosite, magnetite and pyrite. In the oxidation zone minerals such as limonite, wad, psilomelane, goethite and romanèchite were described (Maderspach 1875; Lázár 1959; Grecula et al. 1995; Rojkovič 2000). This article is focused on detailed mineralogical research of the meta-



Legend

Gelnica Group

Bystrý potok Formation (Upper Silurian)

- Quartz-muscovite and graphite-muscovite phyllites
- Quartz phyllites
- Rhyolite metapyroclastics
- Metalidytes
- Metagreywacke
- Metacarbonates

Drnava Formation (Devonian)

- Quartz-muscovite and graphite-muscovite phyllites
- Quartz phyllites
- Quartz metagreywacke
- Rhyolite metapyroclastics



Quaternary

- Proluvial sediments
- Fluvial sediments
- Deluvial sediments

- Locality
- Faults
- Rivers
- Built-up area

Fig. 1 – Geological map of the Betliar-Július manganese occurrence in the Gemeric Unit in the Spišsko-gemerské rudohorie Mts. (modified after Bajaník et al. 1983).

morphosed manganese mineralization at the Betliar-Július occurrence. It provides considerable amount of new data on its mineralogy and constraints on its genesis as well as comparison of the studied locality with the similar localities in the Spišsko-gemerské rudohorie Mts. and the other world occurrences of the metamorphosed manganese ores.

2. Geological settings and localization

Small bodies and lenses of metamorphosed carbonate-silicate manganese ore mineralization are known from the localities Čučma-Čierna baňa, Smolník-Malá Hekerová and Betliar-Július in the Spišsko-gemerské rudohorie Mts. They are hosted in Lower Paleozoic black phyllites and lydites of the Gelnica Group (Gemic Unit) (Fig. 1), metamorphosed in greenschist facies conditions (Kantor 1954; Bajaník et al. 1983; Faryad 1994; Rojkovič 2001; Peterec, Ďud'á 2003). The Gemic Unit is composed of metamorphic Lower Paleozoic basement (Gelnica and Rakovec Group), Upper Paleozoic (Ochtiná, Dobšiná and Gočaltovo Group) and Lower Triassic cover (Kobeliarovo Group) complexes (Bajaník et al. 1983). The Gemic Unit occurs in the hanging wall of the Veporic Unit separated by the Lubeník-Margecany tectonic line. The origin of Lower Paleozoic Gemic basement units is considered as riftogenic associated with active margin of Gondwana (Grecula 1982; Putiš et al. 2008).

The Gelnica Group is metamorphosed formation with polygenetic and polycyclic development with preserved flyschoid sedimentation features and syngenetic acid (rhyolite-dacite) and locally basic volcanism. Metasedimentary complexes are composed of metamorphosed sandstones and pelites, psammites (quartz-muscovitic and graphitic phyllites) with incorporations of metavolcanoclastic material. Metamorphic complexes were intruded by the Permian S-type Gemic granites (Uher, Broska 1996). The Gelnica Group is divided into Vlachovo, Bys-trý potok and Drnava Formations (Bajaník et al. 1983). Lenses of manganese mineralization are situated within metacarbonate bodies of the Bystrý potok Formation presented in ambient graphitic and quartz-muscovitic phyllites with lydites and volcano-sedimentary products (tuffs and tuffites) of synsedimentary basic volcanic activity (Bajaník et al. 1983; Vozárová 1993). Graphitic phyllites and lydites are considered as products of metamorphosed material with organic matter, which is also referred to as metamorphosed black shales (Rojkovič 2001).

The age of the Gelnica Group is determined biostratigraphically to Upper Cambrium-Lower Devonian (Snopková, Snopko 1979) and by U-Pb SHRIMP dating of zircons from rhyolite metavolcanoclastics to the Middle-Late Ordovician range (Vozárová et al. 2017).

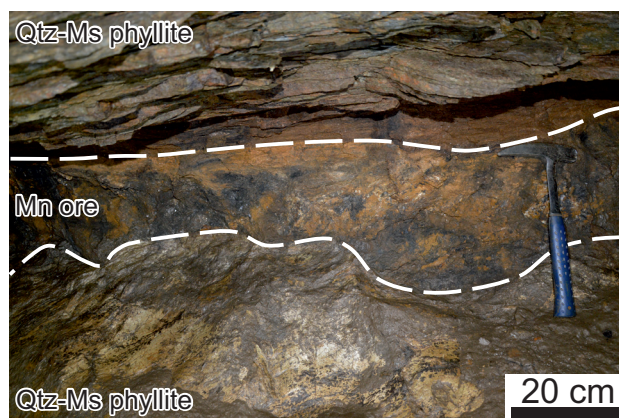


Fig. 2 – Manganese mineralization with oxidized zone in contact with Qtz-Ms phyllites in Roxerová adit at the locality Betliar-Július manganese field.

The Lower Paleozoic complexes of the Gelnica Group were regionally metamorphosed during the Variscan and Alpine tectonic events under the conditions of greenschist facies (Faryad 1991, 1995; Vozárová 1993). The conditions of pre-Alpine metamorphism were determined in the temperature interval of 350–370 °C at the pressure of 3–5 kbar, locally up to 7 kbar (Sassi, Vozárová 1987; Mazzoli, Vozárová 1989; Mysľan, Ružička 2022).

Research on the mineral composition of Mn mineralization was carried out on the locality Betliar on small lenticular bodies, which were excavated since the 19th century at the mining field Július (Maderspach 1875). During further exploration in the 20th century, lenses with Mn ores were discovered in an unnamed (later referred as Roxerová) adit (Fig. 2), with thickness of up to 0.7 m, an inclination of 40–41° (Lázár 1959), located approximately 6 km NW of Rožňava in Spišsko-gemerské rudohorie Mts., Slovakia. The occurrence is situated approximately 1.4 km WSW of the Betliar village on the NE slopes of the Turecká hill (953 m a.s.l.) with GPS coordinates 48°41'53.3"N and 20°29'20.1"E (at altitude 471 m a.s.l.). A system of small exploration pits with fragments of Mn ore can be found directly above the Roxerová adit.

3. Analytical methods

The samples of metamorphosed manganese ores were collected at the dump of the Roxerová exploration adit at the Július mining field near Betliar in 2019. Polished thin sections of ore samples were investigated using a polarised optical microscope Leica DM2500P (Department of Mineralogy, Petrology and Economic Geology, Faculty of Natural Sciences, Comenius University, Bratislava).

Quantitative chemical (WDS) analyses of sulphides were performed using a Cameca SX100 electron microprobe (Department of Mineralogy and Petrology, National Museum, Prague, Czech Republic) and other

minerals were obtained using a JEOL-JXA850F electron microprobe (Earth Science Institute, Slovak Academy of Sciences, Banská Bystrica, Slovakia). The following conditions were applied: accelerating voltage 15 kV, measuring current 20 nA (silicates, oxides, carbonates, phosphates and sulphates) and accelerating voltage 20 kV and measuring current 15 nA (sulphides). The diameter of the electron beam ranged from 1 to 10 μm , PAP/ZAF correction was used. In the silicates and oxides, the following standards and X-ray lines were used: barite (S, $K\alpha$), diopside (Si, Mg, Ca, $K\alpha$), celestine (Sr, $L\alpha$),

orthoclase (K, $K\alpha$), albite (Al, Na, $K\alpha$), barite (Ba, $L\alpha$), hematite (Fe, $K\alpha$), rhodonite (Mn, $K\alpha$), Cr_2O_3 (Cr, $K\alpha$), ScVO_4 (V, $K\alpha$), rutile (Ti, $K\alpha$), apatite (P, $K\alpha$), YPO_4 (Y, $L\alpha$), LaPO_4 (La, $L\alpha$), CePO_4 (Ce, $L\alpha$), NdPO_4 (Nd, $L\alpha$), PrPO_4 (Pr, $L\beta$), EuPO_4 (Eu, $L\alpha$), SmPO_4 (Sm, $L\beta$), TbPO_4 (Tb, $L\alpha$), GdPO_4 (Gd, $L\beta$), ErPO_4 (Er, $L\alpha$), TmPO_4 (Tm, $L\alpha$), DyPO_4 (Dy, $L\beta$), YbPO_4 (Yb, $L\alpha$), HoPO_4 (Ho, $L\beta$), LuPO_4 (Lu, $L\alpha$), LiNbO_3 (Nb, $L\alpha$), UO_2 (U, $M\beta$), ThO_2 (Th, $M\alpha$), tugtupite (Cl, $K\alpha$), fluorite (F, $K\alpha$), crocoite (Pb, $M\beta$), gahnite (Zn, $K\alpha$), Ni_2Si (Ni, $K\alpha$) and Co (Co, $K\alpha$). In the sulphides the following standards and X-ray

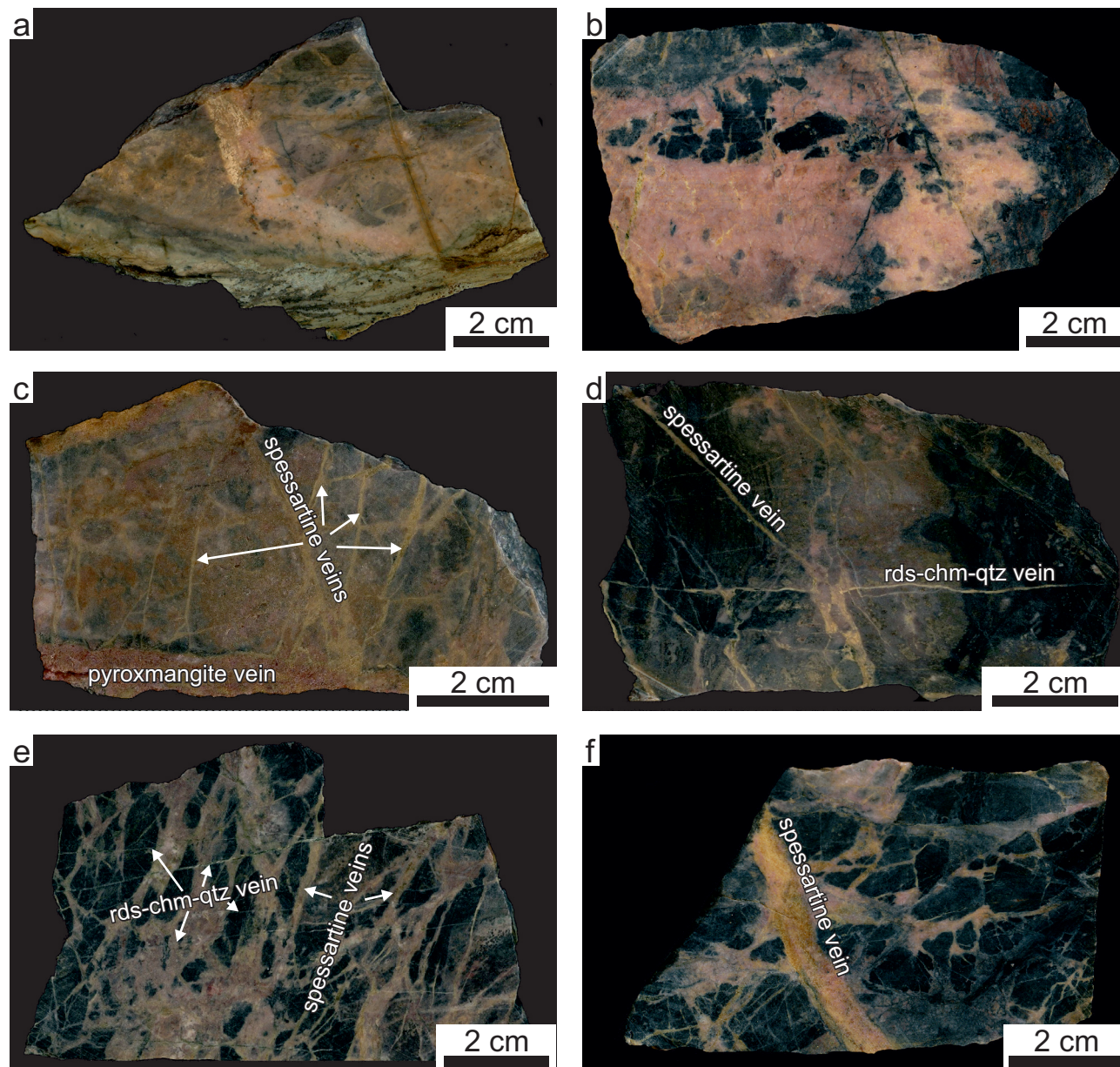


Fig. 3 – Macro view (whole rock scans) of a representative samples with manganese mineralization: **a** – Manganese mineralization in contact with Qtz-Ms phyllite; **b** – Light pink mass composed dominantly by rhodochrosite with magnetite enclaves; **c** – Sample of manganese mineralization intersected by yellow type 2 spessartine veins with a dark pink type 1 pyroxmangite vein (in lower part); **d** – Mn mineralization composed of magnetite and rhodochrosite intersected by yellow type 2 spessartine vein; **e** – Mn mineralization with younger type 3 rhodochrosite-chamosite-quartz veins; **f** – Mn mineralization with thick (up to 7 mm) light yellow type 2 spessartine and type 1 pyroxmangite vein.

lines were used: pyrite (S, Fe, $K\alpha$), chalcopyrite (Cu, $K\alpha$), gersdorffite (Ni, $K\alpha$), cobaltite (Co, $K\alpha$), stibnite (Sb, $L\alpha$), Ag (Ag, $L\alpha$), GaAs (As, $L\beta$) and Bi_2Se_3 (Se, $L\alpha$). The detection limit of every element ranged from 0.002–0.03 wt. %. Elements which were analysed quantitatively and are below the detection limit are not listed in the tables. Photographic documentation of relationships between minerals was carried out in the BSE mode. Abbreviations of minerals are defined in Warr (2021), other abbreviations: BSE – backscattered electrons, XPL – crossed polarized light image.

4. Results

4.1. Primary minerals of manganese mineralization

Manganese mineralization at the Betliar-Július occurrence forms lenticular body embedded in host Qtz–Ms phyllites (Fig. 3a). It consists of fine-grained pink mass (Fig. 3b). The matrix is made dominantly of rhodochrosite, pyroxmangite, spessartine, quartz, minerals of the amphibole supergroup and abundant fine impregnations of magnetite in association with many other less abundant to accessory minerals.

The rhodochrosite-pyroxmangite-spessartine matrix is crosscut by abundant younger veinlets. Three types of intersecting veinlets were distinguished. The oldest type 1 veinlets are up to 1,2 cm thick and consist mainly of pyroxmangite ± spessartine identified in one sample (Fig. 3c), intersected by younger type 2 spessartine veins and the youngest and most common type 3 rhodochrosite-chamosite-quartz veins, with thickness up to 1 cm (Fig. 3b, d, f).

4.1.1. Rhodochrosite

Rhodochrosite is the most abundant mineral in the fine-grained, light pink matrix of the manganese ores. In BSE images, rhodochrosite has no zoning and it is mostly associated with pyroxmangite, spessartine and magnetite (Fig. 4a, b, d). Rhodochrosite is also a dominant mineral in the younger type 3 rhodochrosite-chamosite-quartz veins. It forms anhedral grains and aggregates up to 5 mm in size with no visible chemical zoning (Fig. 4e, f).

Chemical composition of rhodochrosite in the matrix is homogenous (MnCO_3 molecule varies in range of 80.88–91.38 mol. %) and it contains only slightly increased contents of Ca (up to 0.08 *apfu*), Fe^{2+} (up to 0.10 *apfu*) and Mg (up to 0.05 *apfu*), locally with minor Ba, Na and Sr contents (Tab. S1). Chemical composition of rhodochrosite in the veins shows lower content of Mn^{2+} (up to 0.78 *apfu* Mn^{2+} ; 79.06 mol. % MnCO_3) and

higher contents of Ca^{2+} (up to 0.15 *apfu*; 13.08 mol. % CaCO_3) and Fe^{2+} (up to 0.19 *apfu*; 19.63 mol. % FeCO_3) compared to rhodochrosite in the matrix (Fig. 5, Tab. S1).

4.1.2. Pyroxmangite

Pyroxmangite is an abundant mineral which occurs as two types. The first type of pyroxmangite creates elongated euhedral crystals and aggregates in rhodochrosite matrix in association with spessartine and mineral of the amphibole supergroup (Fig. 4a). This pyroxmangite encloses subhedral grains of rhodochrosite (Fig. 4b). The second type of pyroxmangite occurs in up to 1 cm thick type 1 veins (Fig. 4c) with minor presence of spessartine, quartz, rhodochrosite and ferriandrosite-(Ce). Both types of pyroxmangite were also confirmed by powder X-ray diffraction analysis.

Chemical composition of both types of pyroxmangite is shown in a classification diagram (Fig. 6a) with both clearly fitting into the pyroxmangite-type structure field (Fig. 6b). Pyroxmangite in the matrix consists dominantly of Mn (up to 3.90 *apfu*) in *M1*, *M2*, *M3* and *M5* positions with small content of Ca (0.08–0.14 *apfu*) (Tab. S2). The *M4* position is dominantly occupied by Fe^{2+} (0.82–0.93 *apfu*) with a minor content of Mg (up to 0.26 *apfu*) and Mn (up to 0.02 *apfu*). An average ($n = 13$) crystallochemical formula of pyroxmangite from matrix calculated on the basis of 15 oxygen atoms is $(\text{Mn}_{0.87}\text{Ca}_{0.10})_{0.97}(\text{Mn}_{3.01}\text{Fe}_{0.87}\text{Mg}_{0.23})_{4.11}(\text{Si}_{4.96}\text{O}_{15})$. In pyroxmangite from the type 1 veins, crystallochemical positions *M1*, *M2*, *M3* and *M5* are dominantly occupied by Mn (up to 3.92 *apfu*) and position *M4* consists of more Mn (0.31–0.59 *apfu*) and less Fe^{2+} (0.21–0.51 *apfu*) compared to pyroxmangite in the matrix (Tab. S2). Two subtypes of pyroxmangite can be distinguished according to dominant cation in crystallographic position *M4*. Firstly, those with dominant content of Mn (0.43–0.59 *apfu*) over Fe (0.21–0.42 *apfu*) and Mg (0.21–0.29 *apfu*) with average ($n = 17$) crystallochemical formula of pyroxmangite on the basis of 15 oxygen atoms expressed as $(\text{Mn}_{0.87}\text{Ca}_{0.13})_{1.00}(\text{Mn}_{3.50}\text{Fe}_{0.34}\text{Mg}_{0.26})_{4.10}(\text{Si}_{4.95}\text{O}_{15})$. Secondly those, which are characterized by the dominant content of Fe (0.37–0.52 *apfu*) over Mn (0.27–0.44 *apfu*) and Mg (0.20–0.29 *apfu*) with average ($n = 21$) crystallochemical formula of pyroxmangite on the basis of 15 oxygen atoms expressed as $(\text{Mn}_{0.89}\text{Ca}_{0.11})_{1.00}(\text{Mn}_{3.36}\text{Fe}_{0.48}\text{Mg}_{0.24})_{4.09}(\text{Si}_{4.95}\text{O}_{15})$.

4.1.3. Spessartine

Spessartine is an abundant mineral, it occurs in two different environments. Firstly, spessartine forms isolated euhedral crystals, subhedral aggregates and accumulations in rhodochrosite-quartz matrix (Fig. 7a, b). Spessartine contains magnetite, tephroite and pyrosmalite-(Mn)

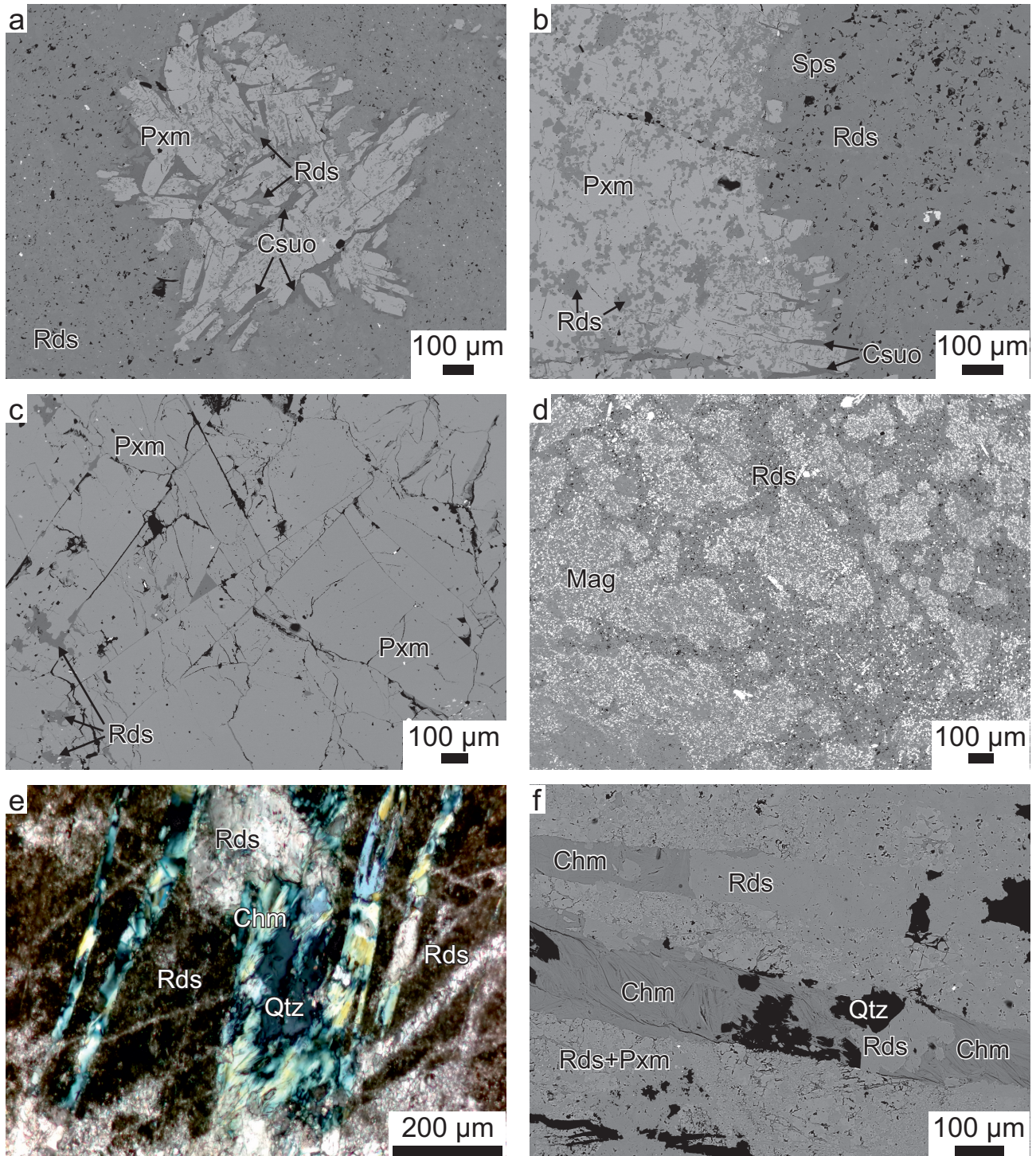


Fig. 4 – BSE images: **a** – Pyroxmangite aggregate in rhodochrosite matrix in association with clino-suenoite; **b** – Detail of pyroxmangite-rhodochrosite contact in matrix with relicts of rhodochrosite in pyroxmangite; **c** – Vein (type 1) pyroxmangite crystals in association with minor rhodochrosite and quartz; **d** – Rhodochrosite matrix with dense impregnation of magnetite grains (white); **e** – Microphotograph of type 3 rhodochrosite-chamosite-quartz veins in manganese ore dominantly composed of rhodochrosite in XPL; **f** – Type 3 rhodochrosite-chamosite-quartz veins in rhodochrosite matrix.

inclusions distributed irregularly in the central or peripheral parts of the garnet crystals (Fig. 7d, e). In XPL spessartine shows strong sector zoning (Fig. 7a). Secondly, spessartine macroscopically forms system of younger

type 2 yellow veins (Fig. 3b, d, f) which intersect rhodochrosite matrix (Fig. 7c). Veins reach size up to 1 cm. Spessartine occurs as aggregates with mostly magnetite and rhodochrosite inclusions (Fig 4c). In spessartine-rich

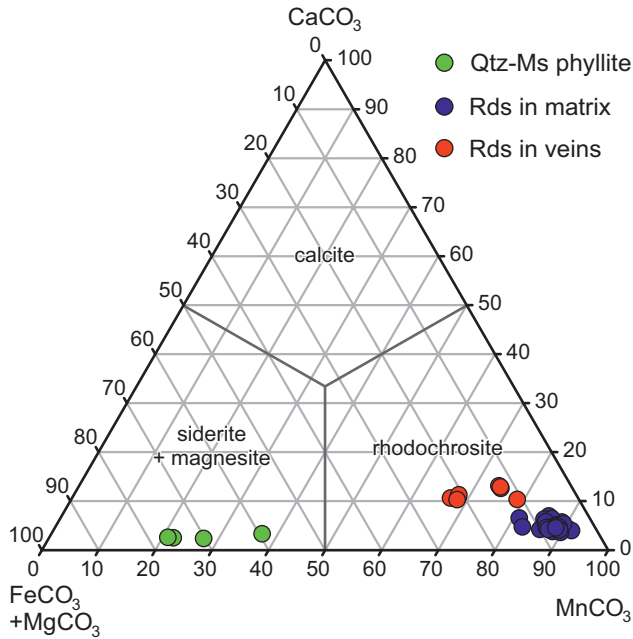


Fig. 5 – The chemical composition of carbonates from Betliar-Július in ternary CaCO_3 –(MgCO_3 + FeCO_3)– MnCO_3 diagram.

matrix parts of samples, replacement of spessartine by rhodochrosite and pyroxmangite was observed (Fig. 7f).

Except of dominant spessartine component (83.93–95.32 mol. %) in spessartine from the matrix, the crystals contain minor almandine (up to 7.83 mol. %), andradite (up to 6.70 mol. %) and grossular (up to 7.42 mol. %) components (Tab. S3). In BSE imaging peripheral zones can be distinguished which are characterized by slightly increased content of Fe^{2+} (up to 0.26 apfu) compared with slightly decreased content of Fe^{2+} (up to 0.10 apfu) in the central parts (Fig. 8, Tab. S3). These spessartines from type 2 veins have similar chemical composition as those in the matrix and dominantly consist of spessartine

molecule (89.67–94.07 mol. %) with minor content of almandine, andradite and grossular molecules (Fig. 8, Tab. S3). They show no chemical zoning in BSE imaging.

4.1.4. Magnetite

Magnetite is one of the most abundant minerals in rhodochrosite matrix rocks where it occurs as accumulations of euhedral to anhedral grains up to 5 μm in size in association with rhodochrosite (Fig. 4d). Significant presence of magnetite impregnations causes macroscopic black colour of Mn ores where it forms aggregates, accumulations and enriched zones. Magnetite accounts for the most common inclusions in the older generation of spessartine with no preferential arrangement in the crystals (Fig. 7e). Magnetite contains slightly increased Mn^{2+} content (up to 0.03 apfu) (Tab. S4).

4.1.5. Minerals of the amphibole supergroup

The amphibole supergroup is represented by clino-suenoite and clino-ferro-suenoite which occur mostly as flattened elongated crystals grouped into fibrous aggregates up to 0.5 mm in size. Amphiboles are present dominantly in the interstitial places between pyroxmangite crystals embedded in rhodochrosite matrix (Fig. 9a, b).

Clino-suenoite and clino-ferro-suenoite form a continuous solid-solution series as shown in a classification diagram (Fig. 10). In clino-suenoite (Tab. S5), the crystallochemical position *A* is fully vacant. The position *B* is occupied by Mn^{2+} (up to 1.87 apfu) with minor content of Ca^{2+} , Ba^{2+} , Na^+ and K^+ . The crystallographic position *C* dominantly consists of Mg^{2+} (up to 2.72 apfu) with lower content of Fe^{2+} (up to 2.33 apfu). Slightly increased content of Mn^{2+} (up to 0.37 apfu), Co^{2+} (up to 0.02 apfu),

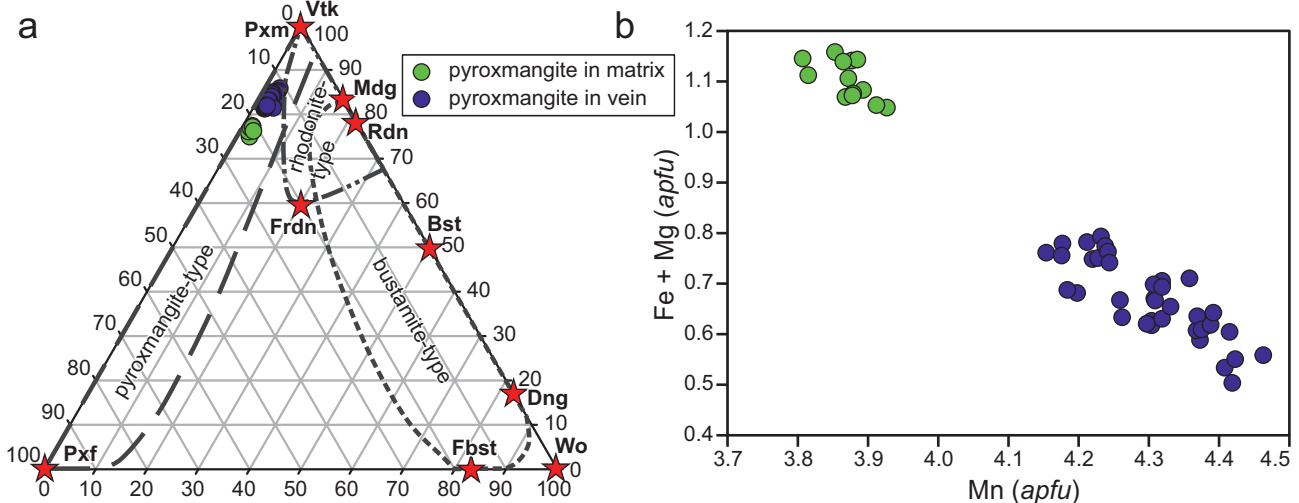


Fig. 6 composition of pyroxenoids from Betliar-Július occurrence: **a** – Classification diagram for pyroxenoids in the Ca–Mn–(Fe+Mg) compositional fields with end-member minerals marked with stars (modified after Shchipalkina et al. 2019a); **b** – Substitution diagram of Mn vs. Fe+Mg (apfu).

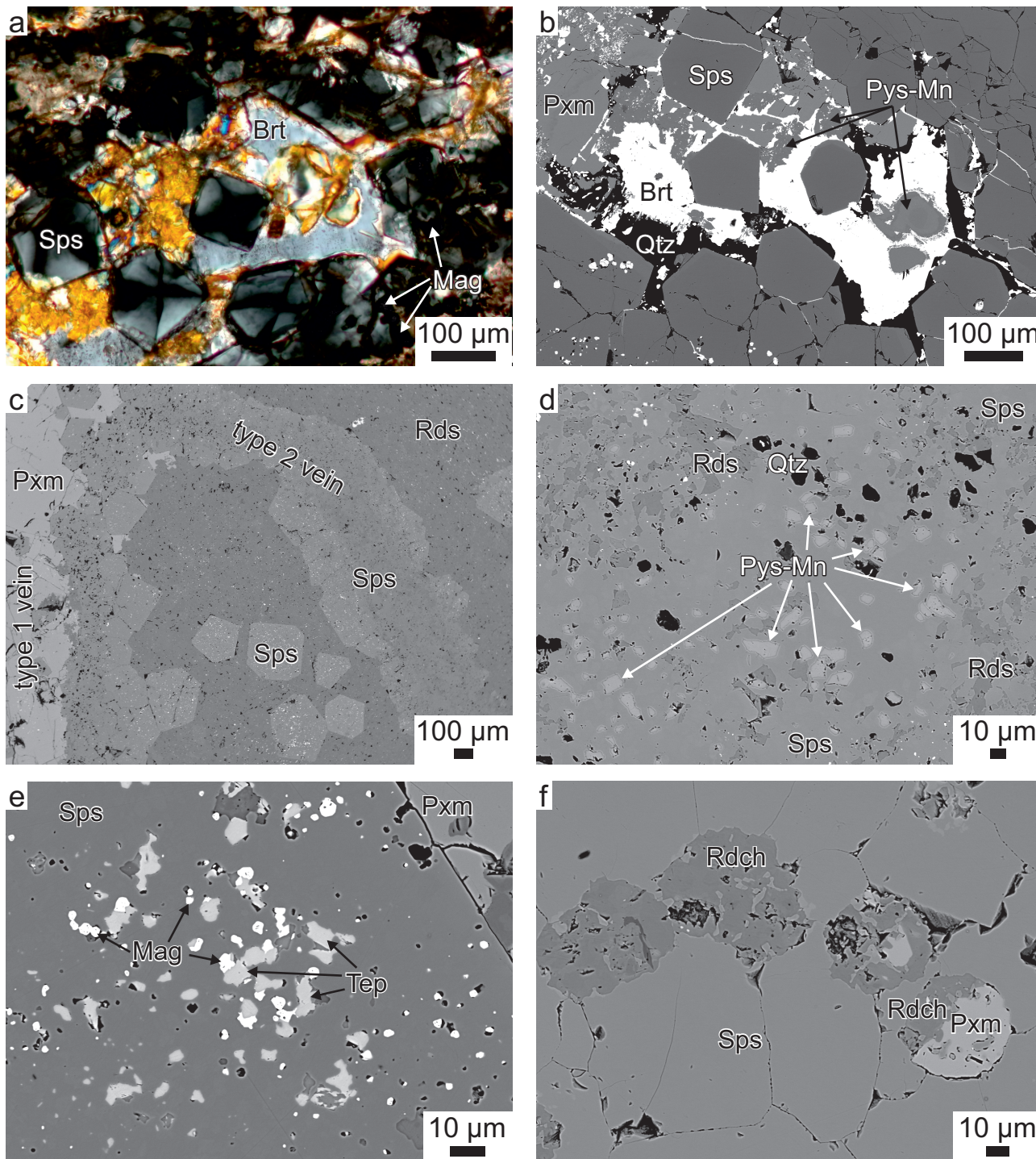


Fig. 7 – appearance of spessartine: **a** – Microphotograph of anisotropic garnets in association with baryte and accessory magnetite in XPL; **b** – Quartz, pyrosmalite-(Mn) and baryte filling the small vug in rhodochrosite matrix with spessartine; **c** – Type 2 spessartine vein intersecting rhodochrosite matrix; **d** – Inclusions of pyrosmalite-(Mn), quartz and rhodochrosite in spessartine; **e** – Tephroite and magnetite inclusions in spessartine; **f** – Spherical replacement of spessartine by rhodochrosite ± pyroxmangite.

Ni^{2+} (up to 0.07 *apfu*) and Zn^{2+} (up to 0.04 *apfu*) can also be observed. Position *W* is dominantly occupied by $(\text{OH})^-$ with minor F^- content (up to 0.11 *apfu*). Chemical composition of clino-ferro-suenoite can be distinguished by

increased content of Fe^{2+} (up to 2.44 *apfu*) and decreased content of Mg^{2+} (up to 2.34 *apfu*) at the crystallographic position *C* (Tab. S5). Content of other constituents at all positions are similar as in clino-suenoite.

4.1.6. Tephroite

Tephroite occurs as common inclusions in spessartine together with magnetite and pyrosmalite-(Mn), where they form subhedral grains approximately 2–10 μm in size (Fig. 7e). Tephroite contains 86.55–89.54 mol. % of tephroite molecule, 8.75–11.09 mol. % of fayalite molecule and 0.93–1.72 mol. % of forsterite molecule (Tab. S6). Other components such as Al, Cr, V, Ni, Ca and Na are only negligible or close to detection limit of microprobe analysis.

4.1.7. Pyrosmalite-(Mn)

Pyrosmalite-(Mn) is rare mineral which forms tabular crystals, subhedral grains and aggregates up to 10 μm in size as inclusions in older generation of spessartine (Fig. 7d) in association with tephroite and magnetite. Due to their small size, no zoning in BSE imaging was observed. Pyrosmalite-(Mn) is also present in vugs filled with quartz and baryte, where it forms subhedral zonal grains 0.1 mm in size (Fig. 7a, b).

The dominant cation in pyrosmalite-(Mn) from matrix is Mn^{2+} (4.80–7.63 *apfu*), less common are Fe^{2+} (0.28–2.95 *apfu*) and Mg^{2+} (up to 0.45 *apfu*). Anion site is dominantly occupied by $(\text{OH})^-$ with minor Cl^- content (up to 1.24 *apfu*) (Tab. S7). In the central parts of pyrophanite crystals situated in vugs, the content of Fe^{2+} (up to 1.48 *apfu*) is lower compared to the content of Fe^{2+} at the edge where it reaches maximum values (up to 2.33 *apfu*). The Mg content indicates a uniform trend. In contrast the Mn content shows opposite trend, where Mn reaches the highest values in the central parts of crystal (up to 6.11 *apfu*) and decreases in the middle part of grains (5.70–6.09 *apfu*) to the minimum (up to 4.85 *apfu* Mn) at the edge (Tab. S7). Substitutional trend between Mn and Fe+Mg shows linear trend (Fig. 11). Baryte aggregates incorporate zonal pyrosmalite-(Mn) crystals, in which disintegration can be observed alongside the edges.

4.1.8. Muscovite

Muscovite is a common mineral in rhodochrosite matrix of ore samples where it forms laminated euhedral to subhedral crystals with significant chemical zoning. It is locally replaced by chamosite. Muscovite has slightly increased content of Fe^{2+} (0.05–0.13 *apfu*), Mg (0.04–0.07 *apfu*) and Mn (0.01–0.05 *apfu*) in *M* position (Tab. S8). The *I* position is dominantly occupied by K (0.63–0.74 *apfu*) with higher content of Na (0.09–0.12 *apfu*) and Ba (0.09–0.23 *apfu*). The lamellar zoning observed in BSE is caused by variable content of Ba which varies from 0.09 *apfu* in dark grey parts to 0.23 *apfu* in lighter parts of crystal (Fig. 9b).

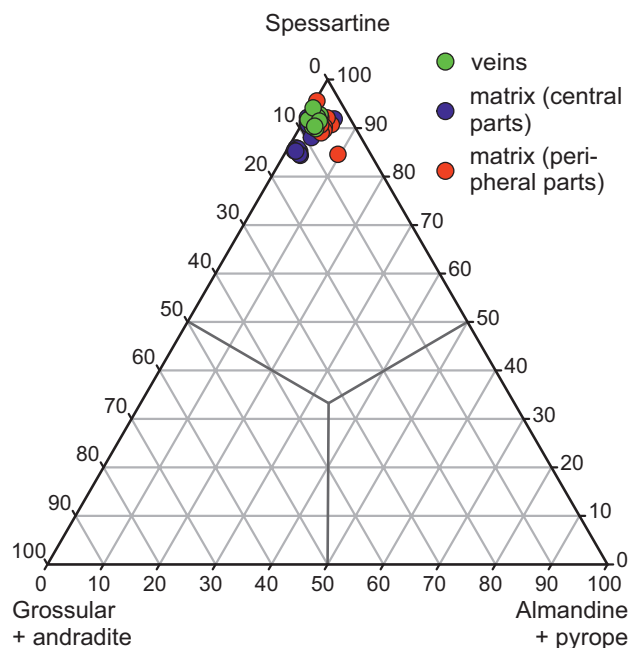


Fig. 8 – Variations in chemical composition of spessartine from Betliar-Július in the classification diagram for garnets.

4.1.9. Baryte

Baryte is a common mineral which fills the interstitial spaces between rhodochrosite, spessartine and pyroxmangite. Baryte is present as an isolated subhedral grains and accumulations of a maximum size up to 0.5 mm (Fig. 7a, b), which are chemically homogenous with only minor presence of Sr^{2+} (up to 0.06 *apfu*) (Tab. S9).

4.1.10. Pyrophanite

Pyrophanite is common accessory mineral embedded dominantly in rhodochrosite matrix where it forms euhedral tabular crystals and aggregates up to 50 μm in size with no visible zoning in BSE. Pyrophanite component is dominantly present in range of 78.75–80.45 mol. % (0.82–0.85 *apfu* Mn^{2+} respectively) with minor ilmenite component in range 19.49–21.00 mol. % (0.21–0.22 *apfu* Fe^{2+} respectively) as show in Tab. S10.

4.1.11. Minerals of the epidote supergroup

Minerals of the epidote supergroup were identified as ferriandrosite-(Ce) and $^{41}\text{Mn}^{2+}$ -analogue of khristovite-(Ce) named vielleaureite-(Ce), both new and recently IMA approved members of this supergroup (Ragu et al. 2023; Števkó et al. 2023). Both occur rarely and were identified in the younger type 1 pyroxmangite vein (Fig. 9c) and in vug in matrix. They have a dark brown colour in PPL and macroscopically form a coarse-grained aggregate. In BSE imaging epidotes form subhedral

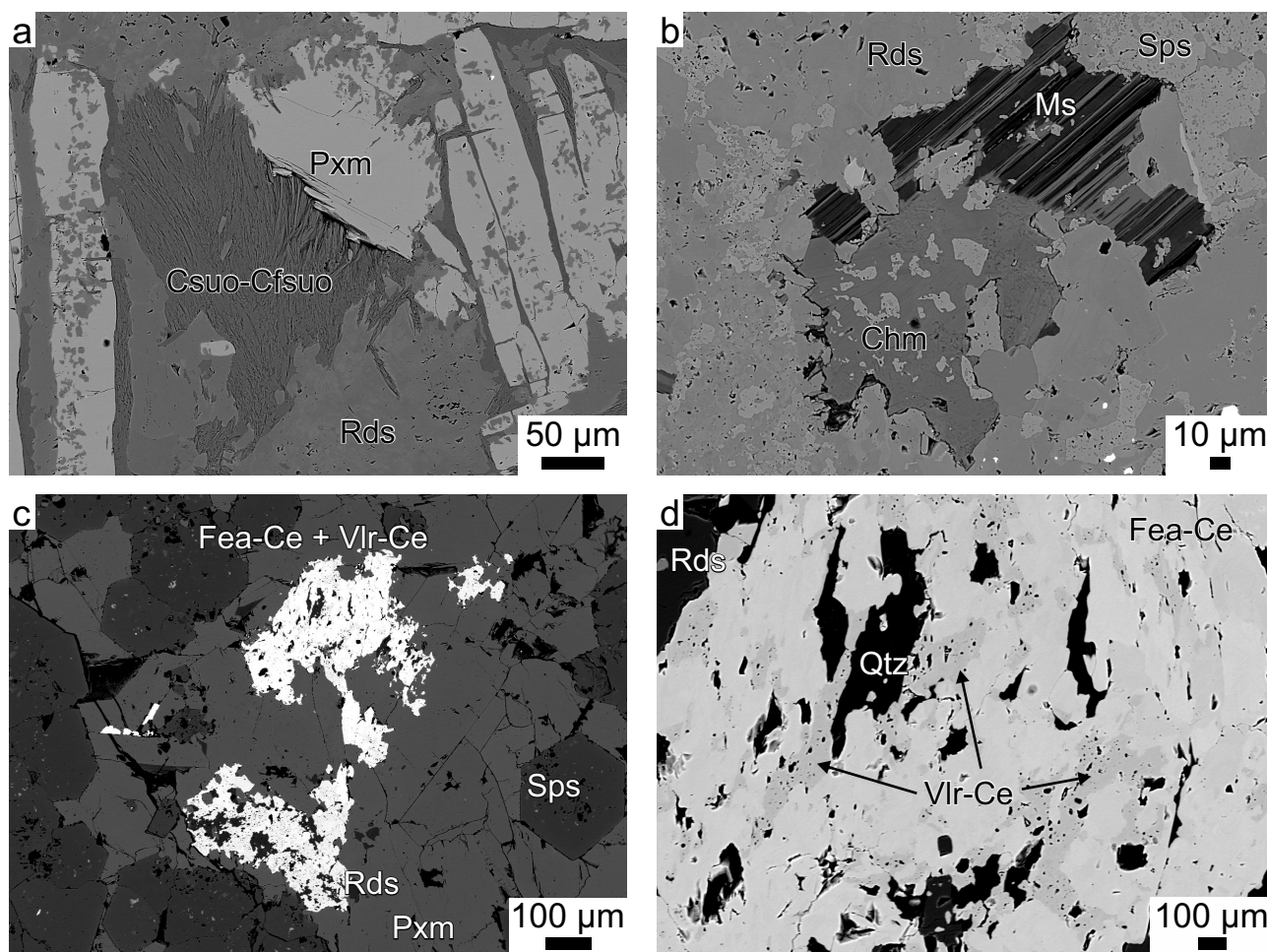


Fig. 9 – BSE images: **a** – Clino-suenoite and clino-ferro-suenoite in association with pyroxmangite crystals in rhodochrosite matrix; **b** – Rhodochrosite–spessartine matrix filled with Ba-rich muscovite locally replaced by chamosite; **c** – Aggregate of epidote supergroup minerals embedded in pyroxmangite–spessartine vein; **d** – Zoning in polycrystalline aggregate composed of the minerals of the epidote supergroup: ferriandrosite-(Ce) (light dark) and vielleaureite-(Ce) (dark grey).

porous grains grouped into aggregate with strong zoning in BSE imaging, where lighter parts are composed of ferriandrosite-(Ce) and darker parts correspond to vielleaureite-(Ce) (Fig. 9d).

Crystallographic positions of ferriandrosite-(Ce) are dominantly occupied as follows: *A1* and *M3* are composed of Mn^{2+} , *A2* by $Y+REE^{3+}$, *M1* consists of Fe^{3+} and *M2* by Al^{3+} (Tab. S11). The content of $Y+REE^{3+}$ varies between 0.89–1.03 *apfu* with dominant Ce^{3+} (up to 0.56 *apfu*), content of Mn^{2+} reaches values up to 1.63 *apfu* and Fe^{3+} up to 1.02 *apfu* with ideal crystallochemical formula expressed as $(Mn^{2+}Ce)(Fe^{3+}AlMn^{2+})O(Si_2O_7)(SiO_4)F(OH)$.

Crystallographic positions of vielleaureite-(Ce) are dominantly occupied in *A1* and *M3* by Mn^{2+} , in *A2* by $Y+REE^{3+}$, in *M1* by Fe^{3+} and *M2* by Al^{3+} (Tab. S11). The content of $Y+REE^{3+}$ is in interval 0.87–0.95 *apfu* with dominant Ce^{3+} (up to 0.51 *apfu*), content of Mn^{2+} reaches values up to 1.67 *apfu* and Fe^{3+} up to 1.02 *apfu*. In addition, in position *O4* content of F^- reaches values in inter-

val 0.51–0.66 *apfu* and therefore we assign this epidote to dollaseite group as a $^{41}Mn^{2+}$ -analogue of khristovite-(Ce) with ideal crystallochemical formula expressed as $(Mn^{2+}Ce)(MgAlMn^{2+})(Si_2O_7)(SiO_4)F(OH)$, recently approved as vielleaureite-(Ce) (Ragu et al. 2023).

4.1.12. Hejtmanite

Hejtmanite is a rare mineral in studied manganese mineralization. It forms an isolated subhedral (Fig. 12b, c) elongated grains up to 20 μm in size embedded in rhodochrosite matrix (Fig. 12a) with no visible zoning in BSE. Chemical composition of hejtmanite is variable (Tab. S12). The *A^p* position is dominantly occupied by Ba^{2+} (1.84–2.24 *apfu*) with minor content of K^+ (up to 0.07 *apfu*), *M^h* position consists of Ti^{4+} (1.90–1.99 *apfu*) and Zr^{5+} (up to 0.10 *apfu*). At the *M^o* position the content of Mn^{2+} reaches values in the range 2.12–2.70 *apfu* with slightly decreased content of Fe^{2+} (1.66–2.17 *apfu*).

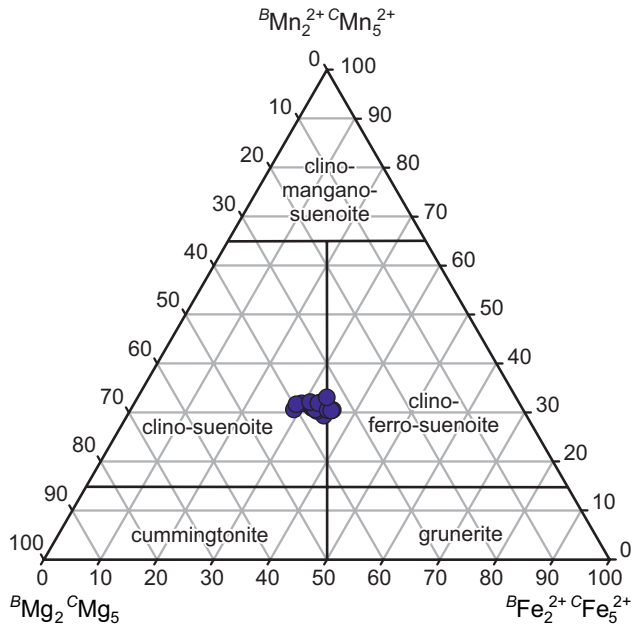


Fig. 10 – Classification diagram for monoclinic Mg–Fe–Mn amphiboles with their compositional boundaries (Hawthorne et al. 2012; Oberti et al. 2018)

The content of Mg^{2+} (up to 0.07 *apfu*) is present at the minimal amount. Anion site is dominantly occupied by $(OH)^-$ (2.60–2.87 *apfu*) with F^- (1.15–2.13 *apfu*). According to WDS analysis of hejtmanite, the continuous transition into bafertisite was observed (Fig. 13) with no visible colour transition in BSE imaging.

4.1.13. Bafertisite

Bafertisite is an extremely rare mineral in studied association, it forms euhedral elongated crystal associated with spessartine, pyroxmangite and rhodochrosite with size approximately $160 \times 20 \mu m$ (Fig. 12d). In bafertisite (Tab. S13) the A^p position is dominantly occupied by Ba^{2+} (2.06–2.23 *apfu*) and M^H position consists of Ti^{4+} (1.97–1.99 *apfu*) and Zr^{5+} (up to 0.03 *apfu*). M^O position is dominantly occupied by Fe^{2+} (2.09–2.40 *apfu*) over Mn^{2+} (2.06–2.22 *apfu*). Content of Mg^{2+} is low (up to 0.07 *apfu*). Anion site is dominantly occupied by $(OH)^-$ (2.68–2.82 *apfu*) over F^- (1.18–1.32 *apfu*). According to WDS analysis of bafertisite, the continuous transition into hejtmanite was observed (Fig. 12d) with no visible transition in BSE imaging.

4.1.14. Fluorapatite

Fluorapatite is an accessory mineral which forms subhedral grains (up to $30 \mu m$ in size) in association with spessartine and pyroxmangite in rhodochrosite matrix, with no visible zoning in BSE imaging. Chemical composition

of apatite is homogenous with low content of REE+Y (up to 0.01 *apfu*). The anion site is fully occupied by F^- (Tab. S14).

4.1.15. Albite

Albite forms anhedral grains in rhodochrosite matrix up to $20 \mu m$ in size. It shows no zoning and has stable chemical composition of almost pure end-member in the interval $Ab_{99.2}$ to $Ab_{99.7}$. Other end-members reach minimum values ($An_{0.2-0.6}$ and $Or_{0-0.2}$) (Tab. S15).

4.1.16. Chamosite

Chamosite forms fibrous crystals grouped to acicular aggregates in association with quartz and rhodochrosite in 0.2 mm thick type 3 veins (Fig. 4e, f). In BSE imaging they show no chemical zoning. Chemical composition of chamosite reflects its dominant content of Fe^{2+} (3.11–3.61 *apfu*) and low contents of Mg (up to 1.15 *apfu*) and Mn (up to 0.33 *apfu*) as shown in Tab. S16.

4.1.17. Quartz

Quartz is one of the most dominant components in rhodochrosite matrix and in quartz–chamosite–rhodochrosite type 3 veins (Fig. 4e, f), where it forms subhedral grains and aggregates.

4.2. Primary sulphidic mineralization

Primary ore mineralization composed of sulphidic minerals is wide-spread in form of isolated euhedral to subhedral grains and aggregates up to 1 mm in size, which are embedded mostly in rhodochrosite matrix. Furthermore,

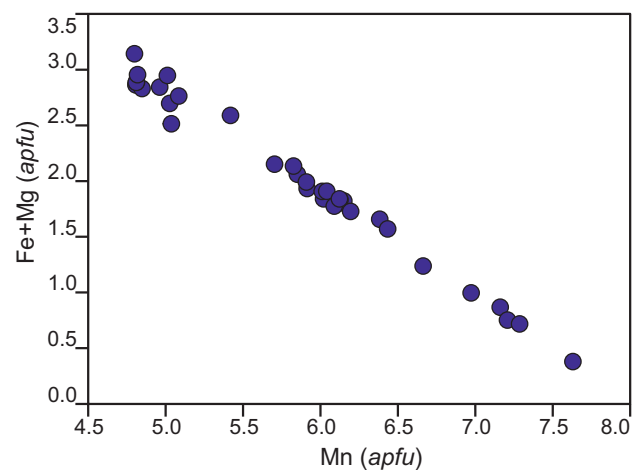


Fig. 11 – Substitution diagram of Mn vs. Fe+Mg (*apfu*) for pyroxmalite-(Mn) from Betliar-Július.

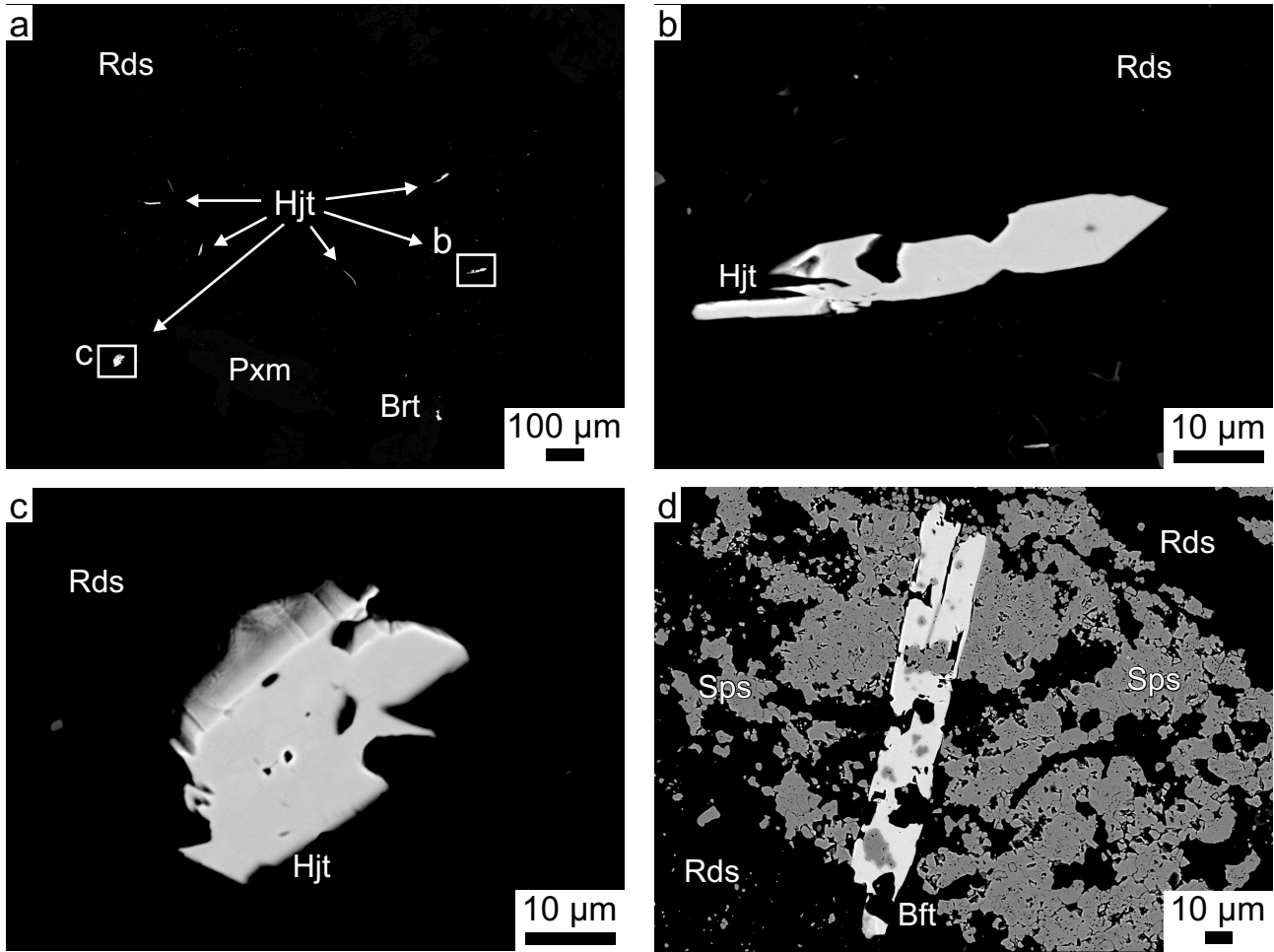


Fig. 12 – BSE images: **a** – Isolated hejtmanite crystals in rhodochrosite matrix; **b** – Elongated hejtmanite crystal in rhodochrosite; **c** – Subhedral grain of hejtmanite in rhodochrosite; **d** – Bafertsite crystal in spessartine–rhodochrosite mass.

near the contact between primary carbonate–silicate Mn mineralization and Qtz–Ms phyllite, a small accumulation of sulphides in the thin layer approximately 2 mm

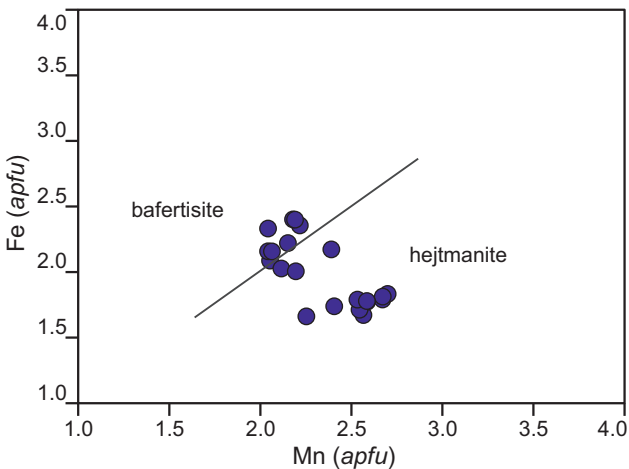


Fig. 13 – Substitution diagram of Fe vs Mn (*apfu*) with classification fields for hejtmanite and bafertsite according to ideal structural formulae of the seidozerite supergroup minerals (Sokolova, Camara 2017).

wide is also present (Fig. 3a, 14a, b). Sulphides are represented dominantly by pyrite, pyrrhotite, chalcopyrite, galena, sphalerite, cobaltite, gersdorffite with minor occurrence of siegenite, violarite, pentlandite and rare millerite (Fig. 14a–f). Pyrite intergrows with pyrrhotite (Fig. 14c). Thiospinels of siegenite–violarite series occur in the form of subhedral crystals (Fig. 14e) 300 µm in size with pentlandite lamellae (Fig. 14f) indicating the exsolution breakdown of a Ni–Co–Fe–S solid-solution phase.

Chemical composition of most sulphides is monotonous with empirical formulae close to ideal end-member composition of individual minerals. An unusual slightly increased content of Mn was observed in pyrite (up to 0.01 *apfu*), chalcopyrite (up to 0.05 *apfu*) sphalerite (up to 0.09 *apfu*) and galena (up to 0.02 *apfu*). Furthermore, Co in pyrite (up to 0.15 *apfu*) and pentlandite (up to 0.07 *apfu*) in matrix alongside with Cu (up to 0.07 *apfu*) were also observed (Tab. S17). Pentlandite lamellae in thiospinels contain higher amount of Co (up to 0.24 *apfu*) (Tab. S18).

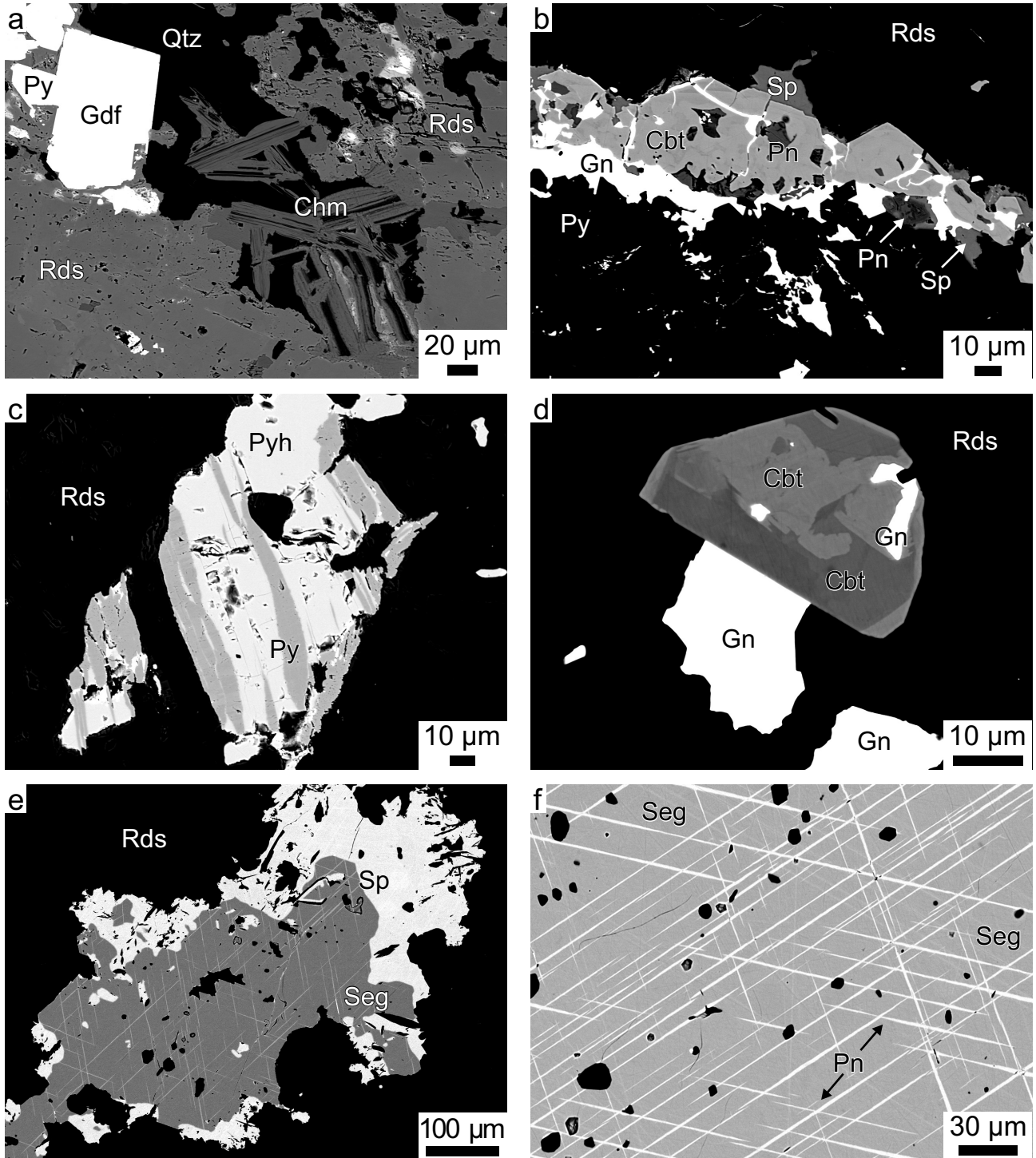


Fig. 14 – BSE images of sulphidic mineralization: a – at the contact of Qtz-Ms phyllite and Mn mineralization; b–f – in rhodochrosite matrix.

In cobaltite subhedral grains (up to 100 µm in size in Fig. 14d, e, f) the higher content of Fe (up to 0.22 *apfu*) in peripherals zones with average (n=26) empirical formulae: $(\text{Co}_{0.73}\text{Ni}_{0.10}\text{Fe}_{0.15})_{\Sigma 1.01}\text{As}_{0.80}\text{S}_{1.19}$ and the lower content of Fe (up to 0.11 *apfu*) in central zones with average (n=20)

empirical formulae: $(\text{Co}_{0.89}\text{Ni}_{0.04}\text{Fe}_{0.06})_{\Sigma 1.02}\text{As}_{0.82}\text{S}_{1.16}$ were observed (Fig. 15). Gersdorffite occurs rarely as an euhedral to subhedral crystals up to 100 µm in size (Fig. 14a) with the average (n=10) chemical composition expressed by empirical formulae: $(\text{Ni}_{0.58}\text{Co}_{0.11}\text{Fe}_{0.31})_{\Sigma 1.01}\text{As}_{1.03}\text{S}_{0.95}$ (Tab. S18).

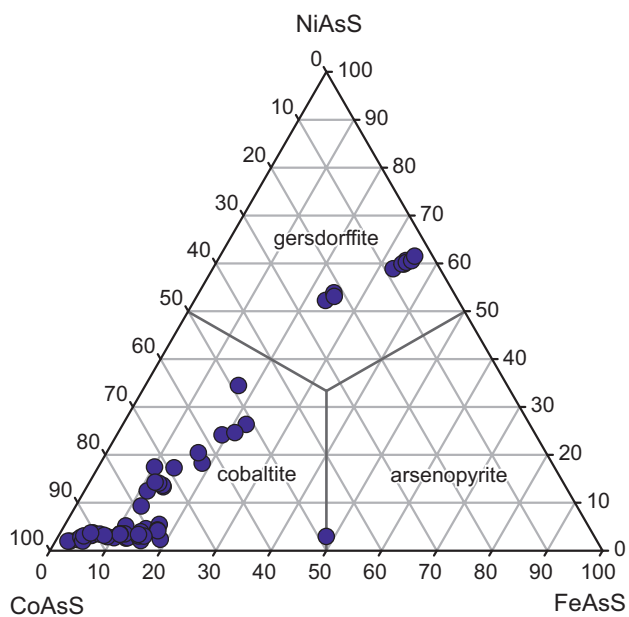


Fig. 15 – The composition of cobaltite and gersdorffite from Betliar-Július in ternary NiAsS–CoAsS–FeAsS system.

4.3. Mineral composition of the host Qtz–Ms phyllite

Phyllites occurs at the contact of manganese mineralization. Macroscopically phyllite has a laminar arrangement and is greyish to light green colour (Fig. 3a). It consists mainly of muscovite and quartz and accessory minerals such as pyrophanite, rutile, zircon and monazite (Fig. 16a, b). At the contact with manganese ore the thin layer of muscovite with chamosite is present with local accumulations of pyrophanite (Fig. 16b). Muscovites have homogenous chemical composition with low contents of Fe^{2+} (0.07–0.10 *apfu*), Mg (up to 0.06 *apfu*) and Mn (up to 0.01 *apfu*) at the *M*-site and low content of Ba (0.01–0.03 *apfu*) at the *I*-site (Tab. S8) with dominant K

(0.81–0.86 *apfu*) and Na (0.10–0.13 *apfu*). Pyrophanite forms euhedral crystals and elongated grains 0.1 mm in size, which overgrows with rutile. Dominant constituent is Ti (0.96–0.98 *apfu*) with MnTiO_3 molecule (up to 79.32 vol. %) and ilmenite molecule (FeTiO_3 , up to 21.95 vol. %) as shown in Tab. S10. Siderite forms a subhedral aggregates (Fig. 16a, b) and consists of FeCO_3 molecule (up to 73.08 mol. %) with slightly higher contents of MnCO_3 molecule (up to 37.23 mol. %), MgCO_3 molecule (up to 6.67 mol. %) and CaCO_3 molecule (up to 3.29 mol. %) as shown in Tab. S1 and Fig. 5

5. Discussion

5.1. Origin of manganese mineralization

Manganese (alongside with iron) in the oceanic sedimentary basins originates in the form of Mn–Fe rich nodules, crusts, cements, mounds and sediment-hosted stratabound layers from multiple processes such as precipitation of elements from hydrothermal fluids and sediment pore waters, hydrogenetic precipitation from seawater and by metasomatic replacement of rocks and sediments (Von Damm 1990; Hein et al. 1997; Usui et al. 2020). Some manganese deposits were created by diagenetic and microbial processes where Mn mostly originated from abiotic processes in the depositional basins and was subsequently oxidized by biological activity of microorganisms (Tebo et al. 2005).

Formation of manganese mineralization in the Spišsko-gemerské rudohorie Mts. was polycyclic and influenced by multiple development stages of a Gemeric Unit. It is assumed that original sedimentary rocks may have been represented by carbonates, clay minerals and quartz. Rojkovič (1999, 2000, 2001) suggested that manganese

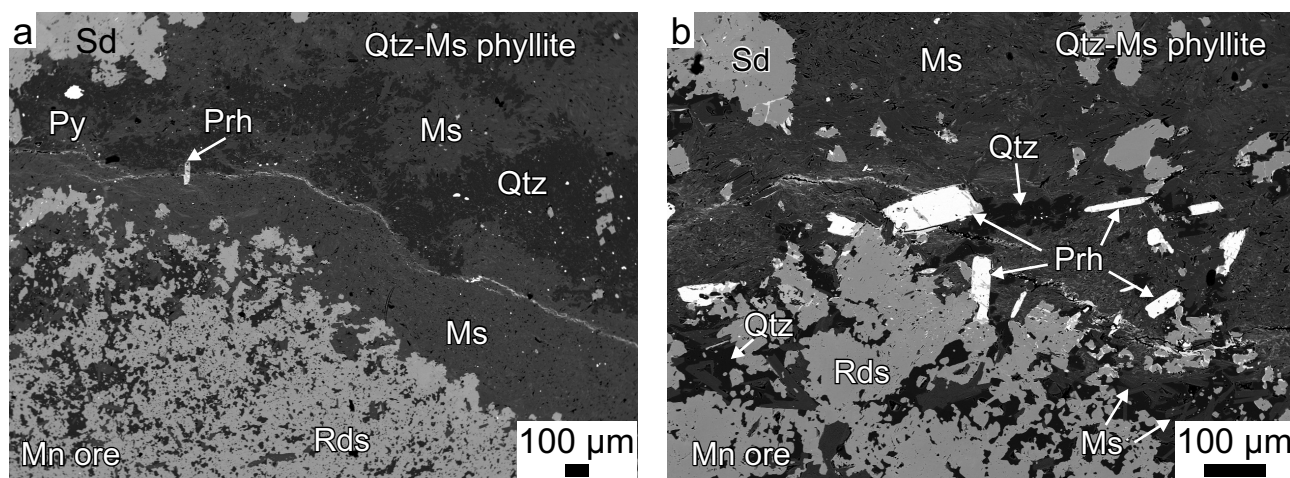


Fig. 16 – Contact of Qtz–Ms phyllite (upper parts of picture) with manganese mineralization in BSE imaging: **a** – Thick muscovite layer between contact of Qtz–Ms phyllite and Mn mineralization; **b** – pyrophanite euhedral crystals at the contact of Qtz–Ms phyllite and Mn mineralization.

was transported from the deep anoxic parts of the ocean into the shallower oxygen-rich waters, where Mn precipitated in the form of manganese oxides and hydroxides. Influence of syngenetic basaltic volcanic activity was suggested by Kantor (1954) and later by Grecula et al. (1995), who assumed that mineralization was formed by volcano-sedimentary processes, accompanied by exhalations of hydrothermal vents, that brought Fe, Mn, SiO₂ and H₂S. Samples from Betliar-Július contain relatively high amounts of Fe suggesting substantial role of submarine volcano-sedimentary fluids of juvenile basaltic volcanism (Ilavský 1957; Grecula et al. 1995) or submarine volcanogenic-exhalative origin (Cornell, Schütte 1995; Mücke et al. 2001; Mücke 2005).

A different view on development of manganese mineralization at the locality Čučma-Čierna baňa was provided by Radvanec, Gonda (2020), who suggest that the major elements (especially Fe, Mn and Ba) were released in the form of fluid phase during anatexis melting of the Silurian rhyolite and Devonian strata-bound sulphidic mineralization.

According to the presence of two generations of minerals with variable chemical composition, we assume that the protolith of Mn mineralization undergone significant changes during the diagenetic stage and was later transformed by intense Variscan and Alpine tectono-metamorphic events, therefore the former protolith of studied manganese mineralization is difficult to interpret. Detailed textural and mineralogical observations lead to construction of paragenetic model of manganese mineralization in Betliar from Variscan to Alpine metamorphism and concurrent hydrothermal activity (Fig. 17).

5.2. Diagenesis and Variscan metamorphic stage

The first stage of metamorphic evolution of the manganese mineralization at the Betliar occurrence is characterized by production of silicates due to high content of quartz and clay minerals in the protolith alongside with decarbonization reactions that happen in rhodochrosite. Rhodochrosite was most likely replaced by pyroxmangite, which might be proven by preserved rhodochrosite relicts in pyroxmangite (Fig. 9a). The contact of rhodochrosite and pyroxmangite is not sharp and locally rhodochrosite transits into pyroxmangite (Fig. 4b). In laboratory conditions, pure pyroxmangite end-member is stable at the temperature of 425–450 °C and 3 kbar pressure (Peters et al. 1973). Stability field of pyroxmangite is enlarged by incorporation of Fe²⁺ and Mg (Maresch, Mottana 1976). Transformation of rhodonite to pyroxmangite occurs at pressure of 3 kbar and temperature approximately 350–400 °C (Maresch, Mottana 1976; Brusnitsyn et al. 2017; Shchipalkina et al. 2019a, b).

Mineral	Metamorphic stage		Hydrothermal phase
	Variscan	Alpine	
Quartz	—	—	
Rhodochrosite	—	—	
Albite	—		
Fluorapatite	—		
Pyrosmalite-(Mn)	—	—	
Magnetite	—		
Tephroite	—		
Pyrophanite	—		
Pyroxmangite	—	—	
Spessartine	—	—	
Muscovite	—		
Hejtanite	—		
Bafertsite	—		
Clino-suenoite	—		
Clino-ferro-suenoite	—		
Baryte		—	
Ferriandrosite-(Ce)		—	
Vielleaureite-(Ce)		—	
Chamosite		—	
Cobaltite			—
Gersdorffite			—
Millerite			—
Pyrite			—
Siegenite			—
Violarite			—
Chalcopyrite			—
Galena			—
Sphalerite			—
Pyrrhotite			—
Pentlandite			—

Fig. 17 – Mineral paragenesis chart for all minerals identified in manganese mineralization from Betliar-Július distributed to pre-metamorphic, metamorphic and hydrothermal stage.

Spessartine was formed by decarbonation and dehydration reactions during the prograde phase of metamorphism, quartz and rhodochrosite inclusions represent residual phases. The low temperature (~300 °C) stability field of spessartine overlaps with the kaolinite stability field, which indicates clay minerals as a precursor of garnets (Nyame 2001). Matthes (1961) claims that pure spessartine is formed at a minimum temperature of 400 °C, but Theye et al. (1996) over all proved, that formation of spessartine starts during the low-pressure prograde metamorphism at ~300 °C. Low content of temperature-dependent cations (such as Ca, Mg and Fe) in spessartine from Betliar indicates low temperatures of equilibration and minimal incorporation of these cations to the garnet structure during the spessartine growth (Nyame et al. 1998; Nyame 2001).

Tephroite could be developed at the expense of rhodochrosite and quartz or pyroxmangite by decarbonation reactions (Mohapatra, Nayak 2003). Tephroite is a common mineral in Mn-rich rocks crystallizing under higher-grade conditions of amphibolite facies with peak conditions reaching 6–7 kbar and 550–700 °C (Santos et al. 2021), but it has also been identified at the localities with lower to upper greenschist facies conditions (e.g. Ashley 1989; Brugger, Gieré 2000; De Putter et al. 2018). Tephroite in

the MnO–SiO₂–H₂O–CO₂ system is stable at mid-grade greenschist facies condition below 420 °C with rhodochrosite and quartz assemblage at low X_{CO_2} (<0.2) (Peters et al. 1973). Pyrosmalite-(Mn) at the Betliar occurrence was probably formed by the hydration and chlorination of the Mn-rich silicates (Stillwell, McAndrew 1957).

Clino-suenoite and clino-ferro-suenoite from Betliar form a continuous solid-solution series (Fig. 10) without a miscibility gap (Oberti et al. 2018). Temperature of amphibole formation is dependent on Mn/(Mn+Mg) values, where range of 400–620 °C for the lower and 570–775 °C at 2 kbar for the upper parts of stability field of pure Mg-Mn clino-suenoite occurs. Incorporation of Fe results in decrease of the stability limits, which is a consequence of a low-grade metamorphic conditions (Melcher 1995).

Rare occurrence of bafertisite and its Mn-analogue hejtmanite (Vrána et al. 1992) was observed in form of isolated crystals (Fig. 12). These minerals occur only on few world localities with manganese mineralization, such as in rhodonite–tephroite–spessartine–quartz association from the Muzeinoe gorge, the Inyl'chek mountain ridge in South-Eastern Kyrgyzstan (Sokolova et al. 2016) or in Fuchs Alps in Austria (Kolitsch et al. 2021). Due to their nominal chemical composition (especially high contents of Ba and Ti) it is assumed that formation of these minerals was conditional on precursor clayey sediments enriched by Ti and Ba. Presence of pyrophanite requires a Mn-Ti rich precursor under low fO_2 conditions (Nayak, Mohapatra 1998). Enrichment of Ti in protolith was probably caused by occurrence of terrigenous admixture (Brusnitsyn 2006). Manganese mineralization at the Betliar occurrence contains relicts of laminated Ba-rich muscovite (Fig. 9b). Formation of muscovite is related to prograde metamorphism of sedimentary clay minerals associated with Ba-rich sediments by dissolution of baryte and precipitation of Ba-rich fluids. The volcanic source of barium at the locality Čučma-Čierna baňa was suggested by Radvanec, Gonda (2020), the synsedimentary source was suggested by Rojkovič (2001).

5.3. Alpine metamorphic stage and hydrothermal activity

The second stage of evolution of manganese mineralization at the Betliar occurrence is characterized by formation of cracks and fissures, filled by younger minerals generated during the Alpine metamorphic stage and hydrothermal phase and recrystallization of meta-stable minerals. In the rhodochrosite matrix, the complex system of younger veins and veinlets occur composed of type 1 pyroxmangite ± spessartine, type 2 spessartine veins and type 3 rhodochrosite–chamosite–quartz veins. The coexistential relationships between individual veins (Fig. 3c–f, 4e, f) shows, that the oldest are type 1 pyrox-

mangite ± spessartine veins, which are cut by younger type 2 spessartine and type 3 rhodochrosite–chamosite–quartz veins. In rhodochrosite (Fig. 5, tab. S1) and spessartine (Fig. 8, tab. S3) the higher content of Fe was observed, concentrations of Fe in vein-type pyroxmangite are lower than in pyroxmangite in the quartz–rhodochrosite matrix (Fig. 6b, tab. S2). Locally, spessartine show slight Fe enrichment in its peripheral parts.

Two members of the epidote supergroup were identified as ferriandrosite-(Ce) and vielleaureite-(Ce). They occur in pyroxmangite type 1 veins or in vugs of quartz–rhodochrosite matrix. Epidotes were formed during the low-grade (greenschist facies) metamorphism with high mobility of REE elements. Similar REE-bearing members of the epidote subgroup were observed at the Veitsch Mn deposit in the upper Austroalpine Greywacke Zone (Girtler et al. 2013). Unequivocal source of REE elements at the Betliar occurrence is difficult to interpret due to their multi-environment origin such as from hydrothermal solutions or from diagenetic processes (Brusnitsyn et al. 2020). Zoning in polycrystalline epidote grains observed in BSE reflects a complicated metamorphic and hydrothermal evolution (Biagioni et al. 2019).

Pyrosmalite-(Mn) has incremental zones (Fig. 7a) in which rising content of Fe and Mg and decreasing content of Mn was observed from the central parts to the peripheral parts of studied crystal. Some authors (Albrecht 1989; Fan et al. 1992) consider pyrosmalite group minerals as a retrograde product of an earlier anhydrous silicates with infiltration of H₂O-rich fluids. Baryte reprecipitated from unstable minerals during the Alpine stage of metamorphism, probably from Ba-rich muscovite which partially recrystallized to Mn-rich chlorite (Fig. 9b).

Occurrence of Ni, Co and Cu-rich sulphides reflects adsorption of these elements in the former sedimentary–diagenetic manganese minerals (Rojkovič 2001) and hydrothermal contribution in the later phase of manganese occurrence evolution. Slightly higher content of Mn is also present in some sulphides (Tab. S17, S18).

Last important part of evolution of Mn mineralization took part due to metasomatic processes, which caused partial recrystallization of spessartine (Fig. 7f), which may have been caused by the circulation of a CO₂-rich fluids as observed by Munteanu et al. (2004).

5.4. Estimation of p–T conditions of Mn mineralization

The most significant feature of Mn mineralization which distinguishes Betliar from the other localities in the Gemeric Unit is absence of a low p–T polymorph of MnSiO₃ (rhodonite), which indicates higher p–T conditions during metamorphic evolution (Peters et al. 1973; Maresch, Mot-

tana 1976). Pressure-temperature conditions estimated in Early Paleozoic rocks of the Gelnica Group compared to stability limits of Mn-amphiboles and incorporation of Fe as suggested by Melcher (1995) indicate formation of these minerals in the lower parts of amphibole stability field at the high-grade greenschist facies conditions.

Pre-Alpine metamorphic conditions estimated from the associating Early Paleozoic metasedimentary and metavolcanic rocks of the Gelnica Group show p–T conditions of greenschist facies at the 300–440 °C and 3–7 kbar (Sassi, Vozárová 1987; Mazzoli, Vozárová 1989; Faryad 1995; Myšľan, Ružička 2022). Rhodonite–pyroxmangite geothermometer of manganese mineralization estimated temperature of 375 ± 10 °C (Faryad 1991), 390 °C (Rojkovič 1999) and 400–420 °C at 3.2–3.7 kbar with $X_{CO_2} = 0.055–0.06$ (Faryad 1994) at the similar locality Čučma-Čierna baňa, what is close to the supposed p–T condition at the locality Betliar-Július.

6. Conclusions

The most abundant minerals at the Betliar-Július manganese occurrence are rhodochrosite, pyroxmangite, spessartine, quartz, magnetite, clino-suenoite, clino-ferrosuenoite, tephroite, pyrophanite, pyrosmalite-(Mn), baryte alongside with pyrite, pyrrhotite, galena, sphalerite, cobaltite, gersdorffite and pentlandite. Less abundant minerals are Ba-rich muscovite, chamosite, albite, fluorapatite and sulphides such as millerite, siegenite and violarite. Very rare minerals are ferriandrosite-(Ce), vielleaureite-(Ce), hejtmanite and bafertisite.

We assume that the protolith was heterogeneous with occurrence of manganese, calcareous, argillaceous and terrigenous material with quartz and Ba-rich minerals locally incorporated by material from a volcanic source. Occurrence of Al-rich clay minerals, quartz and rhodochrosite in precursor sediments during the Variscan metamorphic gradual increase in p–T conditions led to formation of spessartine, tephroite, pyroxmangite, pyrosmalite-(Mn) and other minerals. Abundant occurrence of pyroxmangite and absence of rhodonite suggests, that the mineral assemblage was formed in the p–T conditions approximately 420–450 °C and pressure 2–4 kbar corresponding to the higher grade of greenschist facies. Mn-rich amphiboles were formed at the peak condition of a metamorphism in the high-grade greenschist facies.

Presence of Ba and Ti in precursor sediments provided important source of Ba-/Ti-rich fluids generating Ba-rich muscovite, hejtmanite, bafertisite during Variscan metamorphism and later forming baryte in the Alpine stage.

Alpine metamorphic phase led to formation of veins and veinlets composed of pyroxmangite ± spessartine, spessartine and rhodochrosite–chamosite–quartz. Higher

Fe content might be explained by partial dissolution of magnetite or by reprecipitation of Fe from Fe-rich silicates. At the same time, minerals such as pyrosmalite-(Mn) or epidotes were formed in agreement with lowering temperature of metamorphism with associated higher mobility of REE.

The occurrence of sulphides such as cobaltite, gersdorffite, millerite, siegenite, violarite, pentlandite, chalcopyrite, pyrite, sphalerite and galena indicate a hydrothermal contribution via remobilization and recrystallization of these minerals in the later phase of manganese deposit evolution.

Final stage of metamorphic evolution of Mn mineralization was influenced by metasomatic processes which led to partial replacement of spessartine by rhodochrosite ± pyroxmangite and creation of siderite in associating Qtz–Ms phyllite.

Acknowledgements. We want to thank handling editor Pert Jeřábek for his helpful comments. We are also thankful for the reviews of Juraj Majzlan and Luboš Vrtiška and for their comments which helped us to improve the manuscript. We want to thank Jiří Sejkora for providing us identification of pyroxmangite via X-ray diffraction. This work was financially supported by VEGA project (2/0029/23).

References

- ALBRECHT J (1989) Manganiferous phyllosilicate assemblages: Occurrence, composition and phase relations in metamorphosed Mn deposits. *Contrib Mineral Petrol* 103: 248–241
- ASHLEY P M (1989) Geochemistry and mineralogy of tephroite-bearing rocks from the Hoskins manganese mine, New South Wales, Australia, *Neu Jb Mineral, Abh* 161: 85–111
- BAJANÍK Š, VOZÁROVÁ A, HANZEL V, IVANIČKA J, MELLO J, PRISTAŠ J, REICHWALDER P, SNOPEK L, VOZÁR J (1983) Explanations to geological map of the Slovenské Rudohorie Mts. – Eastern part, 1 : 50 000. ŠGÚDŠ, Bratislava, pp 1–223 (in Slovak)
- BIAGIONI C, BONAZZI P, PASERO M, ZACCARINI F, BALESTRA C, BRACCO R, CIRIOTTI M E (2019) Manganiasakaite-(La) and Ferriakasakaite-(Ce), Two New Epidote Supergroup Minerals from Piedmont, Italy. *Minerals* 9(6): 353
- BRUGGER J, GIERÉ R (2000) Origin and distribution of some trace elements in metamorphosed Fe–Mn deposits, Val Ferrera, Eastern Swiss Alps. *Canad Mineral* 38: 1075–1101
- BRUSNITSYN A I (2006) Mineralogy and Metamorphism Conditions of Manganese Ore at the South Faizulino

- Deposit, the Southern Urals, Russia. *Geol Ore Deposit* 48(3): 193–214
- BRUSNITSYN A I, STARIKOVA E V, ZHUKOV I G (2017) Mineralogy of low grade metamorphosed manganese sediments of the Urals: Petrological and geological applications. *Ore Geol Rev* 85: 140–152
- BRUSNITSYN A I, ZHUKOV I G, LETNIKOVA E F (2020) Geochemistry of Rare and Rare-Earth Elements in Manganiferous Sediments of the Polar Urals and Pai-Khoi. *Lithol Miner Resour* 55(1): 36–54
- CORNELL D H, SCHÜTTE S S (1995) A volcanic–exhalative origin for the world’s largest (Kalahari) Manganese field. *Miner Depos* 30: 146–151
- DASGUPTA S, BANERJEE H, FUKUOKA M, BHATTACHARYA P K, ROY S (1990) Petrogenesis of Metamorphosed Manganese Deposits and the Nature of the Precursor Sediments. *Ore Geol Rev* 5: 359–384
- DE PUTTER T, LIÉGEOIS J-P, DEWAELE S, CAILTEUX J, BOYCE A, MEES F (2018) Paleoproterozoic manganese and base metals deposits at Kisenge-Kamata (Katanda, D.R. Congo). *Ore Geol Rev* 96: 181–200
- FAN D, YANG P (1999) Introduction to and classification of manganese deposits of China. *Ore Geol Rev* 15: 1–13
- FAN D, DASGUPTA S, BOLTON B R, HARIYA Y, MOMOI H, MIURA H, JIAJU I, ROY S (1992) Mineralogy and geochemistry of the Proterozoic Wafangzi ferromanganese deposit, China. *Econ Geol* 87: 1430–1440
- FARYAD S W (1991) Metamorphosis of the sediments of the early Paleozoic of Gemicum Unit. *Miner Slov* 23(4): 315–324 (in Slovak)
- FARYAD S W (1994) Mineralogy of Mn-rich rocks from greenschist facies sequences of the Gemicum, West Carpathians, Slovakia. *Neu Jb Mineral, Mh H* 10: 464–480
- FARYAD S W (1995) Determination of the P–T conditions of the metamorphism of the rock complexes of the Spišsko-gemerské rudohorie Mts. *Miner Slov* 27(1): 9–19 (in Slovak)
- GARGULÁK M, CHMELÍK J, BÖHMER Ľ (1985) Evaluation of Sb-ore forecasts in the Zlatý Stôl-Bystrý potok area. Manuscript, ŠGÚDŠ, Bratislava, pp 1–144
- GIRTLER D, TROPPEL P, HAUZENBERGER C (2013) Androsite-(Ce) and ferriandrosite-(Ce) as indicator for low-grade REE mobility in the Veitsch Mn deposit (Styria). *Mitt Österr Mineral Gesell* 159: 56
- GRECULA P (1982) Gemicum – a segment of the Paleotethys riftogenic pool. *Miner Slov – monograph*, Bratislava, pp 1–263 (in Slovak)
- GRECULA P, ABONYI A, ABONYIOVÁ M, ANTAŠ J, BARTALSKÝ B, BARTALSKÝ J, DIANIŠKA I, DRNZÍK E, ĎUŽA R, GARGULÁK M, GAZDAČKO Ľ, HUDÁČEK J, KOBULSKÝ J, LÖRINCZ L, MACKO J, NÁVESŇÁK D, NÉMETH Z, NOVOTNÝ L, RADVANEC M, ROJKOVIČ I, ROZLOŽNÍK L, ROZLOŽNÍK O, VARČEK C, ZLOCHA J (1995) Mineral deposits of Slovak Ore Mountains. *Miner Slov – monograph*, Bratislava, pp 1–834 (in Slovak)
- HAWTHORNE F C, OBERTI R, HARLOW G E, MARESCH W V, MARTIN R F, SCHUMACHER J C, WELCH M D (2012) Nomenclature of the amphibole supergroup. *Amer Miner* 97(11–12): 2031–2048
- HEIN J R, KOSCHINSKY A, HALBACH P, MANHEIM F T, BAUM M, KANG J K, LUBICK N (1997) Iron and manganese oxide mineralization in the Pacific. *Geological Society of London, Special Publication* 119(1): 123–138
- ILAVSKÝ J (1957) Geology of ore deposits in Spišsko-gemerské rudohorie Mts. *Geol Práce, Zoš* 46: 51–95 (in Slovak)
- KANTOR J (1953a) Manganese deposit on Heckerová (Bytrý potok) west of Smolník. Manuscript, ŠGÚDŠ, Bratislava, pp 1–30
- KANTOR J (1953b) Manganese deposit near Čučma. Manuscript, ŠGÚDŠ, Bratislava, pp 1–32
- KANTOR J (1954) On the genesis of manganese ores in the Spišsko-gemerské rudohorie Mts. *Geol Práce, Zpr*, 1: 70–71 (in Slovak)
- KOLITSCH U, SCHACHINGER T, AUER C (2021) Weitere mineralogische Untersuchungen an dem metamorphen jurassischen Manganvorkommen im Bereich der Fuchsalme in der Hochfeindgruppe, Radstädter Tauern, Salzburg: Nachweise von Arseniolepit, Arsenmedait, Celsian, Coombsit, Fluorcalcioroméit, Gasparit-(Ce), Gasparit-(La), Nd-dominanter Gasparit, Hedyphan, Hejtmanit, Hydrocalcioroméit, Konichalcit, Magnesio-Arfvedsonit, Mimetesit und sein unbenanntes OH-Analogon, Pyrobelonit, Sarkinit, Suzukiit/Bavsiit, Tilasit, Tiragalloit, das unbenannte Epidotgruppenglied $\text{CaSr}(\text{Fe}^{3+}\text{AlMn}^{3+})(\text{Si}_2\text{O}_7)(\text{SiO}_4)\text{O}(\text{OH})$ und weiteren Mineralien. 225–246 In: WALTER F et al. (2021) Neue Mineralfunde aus Österreich LXX, Carinthia II, 211/131: 187–276
- LAZNICKA P (1992) Manganese deposits in the global lithogenetic system: Quantitative approach. *Ore Geol Rev* 7(4): 279–356
- LÁZÁR V (1959) Report on the archive research task „Ankerite stripe Hanková–Volovec in 1959. Manuscript, ŠGÚDŠ, Bratislava, pp 1–82 (in Slovak)
- MADERSPACH L (1875) Die Manganerze von Csucsom und Betlér bei Rosenau im Gömörer Comitate. *Österr Z Berg u, Hüttenwes*, 23: 548–550
- MADERSPACH L (1880) Magyarország vasérc-fekhelyei. Királyi Magyar Természettudományi Társulat Megbi-zásából, Budapest, pp 1–111
- MARESCH W V, MOTTANA A (1976) The pyroxmangite-rhodonite transformation for the MnSiO_3 composition. *Contrib Mineral Petrol* 55: 69–79
- MATTHES S (1961) Ergebnisse zur Granatsynthese und ihre Beziehungen zur natürlichen Granatbildung innerhalb der Pyralpspit-Gruppe. *Geochim Cosmochim Acta* 23: 233–294

- MAZZOLI C, VOZÁROVÁ A (1989) Further data concerning the pressure character of the Hercynian metamorphism in the West Carpathians (Czechoslovakia). *Rc Soc Ital Mineral Petrologia* 43(3): 635–642
- MELCHER F (1995) Genesis of chemical sediments in Birimian greenstone belts: evidence from gondites and related manganese-bearing rocks from Northern Ghana. *Mineral Mag* 59(395): 229–251
- MOHAPATRA B, NAYAK B (2003) Mn-Olivine from Gangpur Group of Rocks, Orissa. *J Geol Soc India* 61: 581–587
- MUNTEANU M, MARINCEA S, KASPER H U, ZAK K, ALEXE V, TRANDAFIR V, SAPTEFRATI G, MIHALACHE A, (2004) Black chert-hosted manganese deposits from the Bistritei Mountains, Eastern Carpathians (Romania): petrography, genesis and metamorphic evolution. *Ore Geol Rev* 24(1–2): 45–65
- MÜCKE A (2005) The Nigerian manganese-rich iron-formations and their host rocks – from sedimentation to metamorphism. *J Afr Earth Sci* 41(5): 407–436
- MÜCKE A, MOHAPATRA B K, NAYAK B (2001) The tephroite, spessartine, pyroxmangite and rhodochrosite-bearing mineral assemblages of the manganese ores in the Manamunda–Goriajhar area of the Gangpur Group, India. Petrological and chemical investigation and their genetic implications. *Neu Jb Mineral, Abh* 176: 21–43
- MYŠĚAN P, RUŽIČKA P (2022) Micas and chlorites as indicators of metamorphic conditions of carbonate rocks of the Gelnica Group in the Southern Gemicum (Slovak Republic). *Bull Mineral Petrolog* 30(1): 108–123 (in Slovak)
- NAKAGAWA M, SANTOSH M, MARUYAMA S (2009) Distribution and mineral assemblages of bedded manganese deposits in Shikoku, Southwest Japan: Implications for accretion tectonics. *Gondwana Res* 16: 609–621
- NAYAK B R, MOHAPATRA B K (1998) Two morphologies of pyrophanite in Mn-rich assemblages, Gangpur Group, India. *Mineral Mag* 62(6): 847–856
- NYAME F K (2001) Petrological significance of manganese carbonate inclusions in spessartine garnet and relation to the stability of spessartine in metamorphosed manganese-rich rocks. *Contrib Mineral Petrol* 141: 733–746
- NYAME F K, KASE K, YAMAMOTO M (1998) Spessartine Garnets in a Manganiferous Carbonate Formation from Nsuta, Ghana. *Resour Geol* 48: 13–22
- OBERTI R, BOIOCCHI M, HAWTHORNE F C, CIRIOTTI M E, REVHEIM O, BRACCO R (2018) Clino-suenoite, a newly approved magnesium–iron–manganese amphibole from Valmalenco, Sondrio, Italy. *Mineral Mag* 82(1): 189–198
- PETEREC D, ĎUŽA R (2003) Rare minerals of Mn deposit near Čučma. *Natur Carp* 44: 229–236 (in Slovak)
- PETEREC D, ĎUŽA R (2009) Manganese mineralization at the locality Čučma. *Minerál* 17(5): 410–414 (in Slovak)
- PETERS T J, SCHWANDER H, TROMMSDORFF V (1973) Assemblages among tephroite, pyroxmangite, rhodochrosite, quartz: experimental data and occurrences in the Rhaetic Alps. *Contrib Mineral Petrol* 42: 325–332
- PUTIŠ M, SERGEEV S, ONDREJKA M, LARIONOV A, SIMAN P, SPIŠIAK J, UHER P, PADERIN I (2008) Cambrian–Ordovician metaigneous rocks associated with Cadomian fragments in the West-Carpathian basement dated by SHRIMP on zircons: A record the Gondwana active margin setting. *Geol Carpth* 59: 3–18
- RADVANEČ M, GONDA S (2020) Successive formation of Fe and Mn skarns in the Čučma locality (Gemic unit, W. Carpathians): from metasomatic stage through the amphibolite facies overprint with Ti-rich tephroite to retrograde stilpnomelane–chlorite zone. *Miner Slov* 52(2): 103–132
- RAGU A, BINDI L, BONAZZI P, CHOPIN C (2023) Vielleaureite-(Ce), IMA 2022-134. *CNMNC Newsletter* 72; *Mineral Mag* 87: 1–7
- ROJKOVIČ I (1999) Manganese mineralization in the Western Carpathians, Slovakia. *Geol Carp, special issue* 50: 191–192
- ROJKOVIČ I (2000) Mineralogical characteristics of manganese ores in Slovakia. Appendix of the final report Metallogenetic assessment of the territory of the Slovak Republic. Manuscript, ŠGÚDŠ, Bratislava, pp 1–158 (in Slovak)
- ROJKOVIČ I (2001) Early Paleozoic Manganese ores in the Gemicum Superunit, Western Carpathians, Slovakia. *Geolines* 13: 34–41
- SANTOS F H, AMARAL W S, KONHAUSER K, MARTINS D T, CASTRO M P, QUEIROGA G N, CHI-FRU E, ANDERSEN M B (2021) Unraveling sedimentary precursors and metal enrichment of high-grade metamorphosed manganese rich rocks from the Borborema Province, northeastern Brazil. *Ore Geol Rev* 137: 104283
- SASSI R, VOZÁROVÁ A (1987) The pressure character of the Hercynian metamorphism in the Gemicum (West Carpathians, Czechoslovakia). *Rend Soc Ital Min Petr* 42: 73–81
- SHCHIPALKINA N V, PEKOV I V, CHUKANOV N V, BIAGIONI C, PASERO M (2019a) Crystal chemistry and nomenclature of rhodonite-group minerals. *Mineral Mag* 83(6): 829–835
- SHCHIPALKINA N V, PEKOV I V, CHUKANOV N V, ZUBKOVA N V, BELAKOVSKIY D I, BRITVIN S N, KOSHYLYAKOVA N N (2019b) Vittinkiite, $MnMn_4[Si_5O_{15}]$, a new member of rhodonite group with a long history: definition as a mineral species. *Mineral Mag* 84(6): 869–880
- SNOPKOVÁ P, SNOPKO L (1979) Biostratigraphy of the Gelnica series in the Spišsko-gemerské rudohorie Mts. based on palynological results (Western Carpathians, Paleozoic). *Western Carpathians ser Geol* 5: 57–102 (in Slovak)
- SOKOLOVA E, CÁMARA F (2017) The seidozerite supergroup of TS-block minerals: nomenclature and classification, with change of the following names: rinkite to rinkite-

- (Ce), mosandrite to mosandrite-(Ce), hainite to hainite-(Y) and innelite-1 *T* to innelite-1*A*. *Mineral Mag* 81(6): 1457–1484
- SOKOLOVA E, CÁMARA F, HAWTHORNE F C, PAUTOV L A (2016) From structure topology to chemical composition. XX. Titanium silicates: the crystal structure of hejtmanite, $\text{Ba}_2\text{Mn}_4\text{Ti}_2(\text{Si}_2\text{O}_7)_2\text{O}_2(\text{OH})_2\text{F}_2$, a Group-II TS-block mineral. *Mineral Mag* 80 (5): 841–853
- STILLWELL F L, MCANDREW J (1957) Pyrosmalite in the Broken Hill lode, New South Wales. *Mineral Mag* 31(236): 371–380
- ŠTEVKO M, PLECHÁČEK J, VENCLÍK V, MALÍKOVÁ R (2015) Hausmannite a manganosite from the Čučma-Čierna baňa manganese deposit (Slovak Republic). *Bull mineral-petrolog Odd Nár Muz, Praha* 23(1): 39–42
- ŠTEVKO M, MYŠĽAN P, BIAGIONI C, MAURO D, MIKUŠ T (2023) Ferriandrosite-(Ce), a new member of the epidote supergroup from Betliar (Slovakia). *Mineral Mag* 87: 887–895
- TEBO B M, JOHNSON H A, MCCARTHY J K, TEMPLETON A S (2005) Geomicrobiology of manganese(II) oxidation. *Trends Microbiol* 13: 421–428
- THEYE T, SCHREYER W, FRANSOLETT A M (1996) Low-temperature, low-pressure metamorphism of Mn-rich rocks in the Lienne Syncline, Venn-Stavelot Massif (Belgian Ardennes) and the role of carpholite. *J Petrol* 37: 767–783
- UHER P, BROSKA I (1996) Post-orogenic Permian granitic rocks in the Western Carpathian–Pannonian area: Geochemistry, mineralogy and evolution. *Geol Carpath* 47: 311–321
- USUI A, HINO H, SUZUSHIMA S, TOMIOKA N, SUZUKI Y, SUNAMURA M, KATO S, KASHIWABARA T, KIKUCHI S, URAMOTO G I, SUZUKI K, YAMAOKA K (2020) Modern precipitation of hydrogenetic ferromanganese minerals during on-site 15-year exposure test. *Sci Rep* 10(1): 3558
- VRÁNA S, RIEDER M, GUNTER M E (1992) Hejtmanite, a manganese-dominant analogue of bafertsite, a new mineral. *Eur J Mineral* 4: 35–43
- VON DAMM K I (1990) Seafloor hydrothermal activity: black smoker chemistry and chimneys. *Annu Rev Earth Planet Sci* 18: 173
- VOZÁROVÁ A (1993) Variscan metamorphism and crustal evolution in Gemicum Unit. Western Carpathians ser miner petrogr geochem metalog 16: 55–117 (in Slovak)
- VOZÁROVÁ A, RODIONOV N, ŠARINOVÁ K, PRESNYAKOV S (2017) New zircon ages on the Cambrian–Ordovician volcanism of the Southern Gemicum basement (Western Carpathians, Slovakia): SHRIMP dating, geochemistry and provenance. *Int J Earth Sci* 106: 2147–2170
- WARR L N (2021) IMA-CNMNC approved mineral symbols. *Mineral Mag* 85: 291–320